Published in: Packaging Technology and Science 2017, DOI: 10.1002/pts.2298

An industry oriented strategy for the finite element simulation of paperboard creasing and folding

Marco Domaneschi[a], Umberto Perego[a], Eric Borgqvist[b], Roberto Borsari[c]
[a]Politecnico di Milano, Dept. Civil and Environm. Engng., Milano, Italy
[b]Tetra Pak Packaging Solutions AB, Lund, Sweden
[c]Tetra Pak Packaging Solutions S.p.A., Modena, Italy

Abstract

The numerical simulation of paperboard creasing and folding processes is of increasing importance for the design and production of safe and reliable packaging systems. The extreme material anisotropy and the complexity of these processes require however simulation capabilities which are seldom available in commercial codes. Several approaches have been proposed in the literature over the years, in most cases making use of nonlinear material models developed ad hoc for this purpose. These models, some of which are very effective and accurate, are not in general available in commercial codes and are often based on the definition of a large number of parameters. In this paper, the possibility to obtain acceptable, first hand simulation results using only features already available in a commercial code is investigated. An advanced continuum constitutive model, recently presented in the literature, has been used as a reference for tuning the model and for assessing its accuracy. It is shown how standard features, usually available in state-of-the-art commercial codes, can be employed to deal with the extreme material anisotropy, obtaining qualitatively good results in both the creasing and folding phases. The used standard model accounts for the extremely high anisotropy by means of embedded shell elements, playing the role of reinforcements in the fiber direction. The matrix is assumed to be isotropic and elastoplastic, with properties determined based on the behavior in the thickness direction. The adopted plasticity model, is a modified Drucker-Prager model with a cutoff on the tensile pressure side, available in the used commercial code. The procedure adopted for the identification of the small number of required material parameters is also discussed.

Keywords: creasing, folding, continuum, optimization, embedment

1. Introduction

In industrial paperboard packaging, the final package shape is achieved by folding the paperboard flat blank around predetermined lines, usually called creasing-lines. The final quality of the package is affected by the creasing-folding procedure, which is expected to produce uniform, well-defined, undamaged edges and corners. To facilitate paperboard folding, the paperboard blank is creased before being converted into its final shape, i.e. the folding lines are scored onto the paperboard by pressing it into a grooved female die by a male die with a rule.

Typical results of physical creasing and folding tests on paperboard are shown in Figure 1. A local, shear-induced damage is produced into the paperboard structure during the preliminary creasing phase, which reduces the transverse cohesion between paperboard layers, facilitating the subsequent delamination during the folding phase. During folding, the compressed paperboard layers buckle and are expelled from the bulk material through delamination, dramatically reducing the bending stiffness (Figure 1b), thus facilitating a clean folding around the crease lines. The final result of the creasing and folding processes depends on several factors: i.e. paperboard structure and properties, size and shape of the creasing tools, process speed and other production parameters which are set in the converting factory. The optimal combination of these parameters can be decided either by a trial and error physical approach, where final packages produced with

different settings are examined, or by a virtual approach, by means of advanced numerical simulations. In the latter case, robust and computationally effective finite element models represent an essential tool.

The standard industrial process for the production of packaging paperboard consists of spraying a cellulose fiber water suspension on a moving web. The result of this procedure is the stratification of fibers, typically 1-3 mm long and 10-50 μm thick, in the form of an anisotropic network, giving rise to a board of typical thickness of 0.2-0.5 mm and of density 300-900 kg/m^3. The fibers turn out to be disposed in layers, with most fibers oriented along the machine direction (MD), a smaller portion along the cross machine direction (CD) and, finally, only few in the thickness one (ZD). As a result, the paperboard shows highly anisotropic, but substantially orthotropic properties along MD, CD and ZD directions. Usually MD is the strongest and stiffest one, about 1-5 times with respect to CD. Conversely, ZD results the weakest and most deformable, with strength and stiffness reductions of the order of 100 times the corresponding values in MD, and with an unsymmetrical tension-compression response.

Paperboard can be produced in the form of single ply or multi-plies. This last arrangement usually consists of a sandwich structure, with stronger outer layers that allow improving the overall mechanical performance in bending with a light-weight structure. These extreme material features need be combined with the mechanical complexity of the creasing and folding processes, which involve large strain plasticity, damage, nonlinear geometric response with buckling, contact and self-contact.

Several different models have been presented in the literature for the simulation of paperboard behavior. Kulachenko and Uesaka (2012) [15] modeled paperboard as a fiber network, with fibers modeled as beam elements, thus reproducing the material microscopic structure. Models of this type, though useful for understanding the influence of phenomena occurring at the microscale, are obviously not suited for an effective simulation of the complete creasing-folding process at the macroscale.

The modelling of paperboard as a hybrid continuum, with a discrete number of cohesive interfaces through ZD, has been one of the most popular modelling choices, intended to deal with the extreme anisotropy in ZD. The cohesive interfaces define pre-determined delamination sites, where the material weakness in ZD is localized, and the finite element mesh need be designed to incorporate them. The material layers between two subsequent interfaces exhibit only a mild anisotropy, which can be treated with standard elastoplastic material models. A large number of parameters is usually required to characterize both the continuum and the interface models. This solution, even if straightforward, has limited applications in an industrial environment due to the unrealistic localization of damage along predetermined planes and the large number of parameters to be defined.

One of the earliest hybrid models for paperboard has been proposed in Xia (2002) [24] where an in-plane elastoplastic model, with elastic behavior in the thickness direction, for the simulation of the in-plane behavior (Xia et al., 2002) [25], has been coupled to an interface model, intended to reproduce the damaging out-of-plane behavior in creasing and folding. Beex and Peerlings (2009) [2] followed a similar approach, proposing a continuum model with cohesive interfaces, allowing for delamination between well-identified paper plies. A Hill orthotropic hardening plasticity criterion together with linear elastic anisotropic behavior was assumed for the continuum model. The delamination model was based on Ortiz and Pandolfi (1999) [22] cohesive model. Although the material and delamination models were both relatively simple, comparisons with experimental data showed that the model could predict the paperboard response with acceptable accuracy, with both multiple delamination and plasticity taking place in the shear regions during creasing. Nygårds et al. (2009) [20] discussed the FE analysis of a multi-ply paperboard subjected to creasing by a laboratory device. Also in this case, in-plane and out-of-plane behaviors were assumed to be decoupled. The multi-ply paperboard was modeled as a multilayered structure with cohesive softening interfaces connecting the paperboard plies. An anisotropic elastic–plastic constitutive law, based on the work of Xia et al. (2002) [25], was used to model the paperboard matrix. The simulations were in good agreement with experimental

results. Paperboard properties, such as out-of-plane shear and compression, friction between the paperboard and the creasing device, turned out to have a critical influence on the response. Further studies were carried out in (Huang and Nygårds 2010 [12], Huang and Nygårds 2011 [13] and Huang et al. 2014[14]). Three multi-ply paperboard strips were studied both experimentally and numerically, in both MD and CD directions (see Figure 2 for the definition of material directions). A FE model reproducing the experimental creasing and folding setup was developed, and the creasing and folding behavior was satisfactorily predicted. It was shown that the interface strength mainly affects the folding behavior, whereas the ply properties have more influence on the response during creasing. A similar approach, with three paperboard layers, modeled by means of Hill's anisotropic yield criterion and separated by cohesive interfaces, was also adopted in Li et al. (2014) [16]. A study on the delamination properties of paperboard layers has been recently proposed in Li et al. (2016) [17].

A completely different approach based on a shell model, with damaging line hinges for the folding simulation of pre-creased paperboard, has been proposed in (Giampieri et al. 2011) [8], for application to large-scale computations of package forming processes. The creasing process has not been modeled. A simplified material model for the crease lines behavior has been formulated at the macroscale in terms of generalized variables, aiming at computational effectiveness. Only few parameters are needed to characterize the model, as it is desirable for simulations of overall forming processes in industrial environment.

As an alternative to the hybrid models discussed above, a continuum large strain orthotropic 3D plasticity model has been proposed in (Borgqvist et al, 2014, 2015) [3][4]. In this case, there are no cohesive interfaces through the paperboard thickness and localized delamination is not accounted for. Damage propagation is simulated only through the development of localized plastic deformations in some regions of the board. The preferred directions of the material are represented by three vectors, with the out-of-plane vector transforming as a normal vector rather than as a line segment, allowing for a decoupling of the in-plane and the out-of-plane responses in shearing, during the creasing process. The model is formulated in a large strain framework, based on an orthotropic free energy potential and a multiplicative decomposition of total strains in the plastic regime. An expression for the plastic spin is proposed capable to provide an enhanced shearing in thickness direction. The material model is implemented in the finite element code Abaqus [1] in the form of a user subroutine. Creasing processes obtained by both the simplified line crease setup and the actual rotation crease setup used in industrial applications are studied. The capability of the model in predicting the folding process has also been investigated in (Borgqvist et al 2016)[5].

The main objective in the design of a large scale industrial creasing process is to achieve robustness, i.e. to identify a suitably large region of stable and repeatable operations in the process parameters space. The relevant parameters are paperboard properties (elasticity and elongation, tensile/compression strength, bending behaviour, delamination strength, …), creasing tools geometry and process parameters. The availability of robust models capable to capture the main features of the creasing and folding processes and to converge even in complex loading scenarios has the great value to effectively support risk analysis related to process design and setup, as well as to enable sensitivity analyses on the effect of different parameter combinations on the overall response. Accuracy requirements, while being of course important, can be relaxed if models can still drive qualitative/semi quantitative assessments on the paperboard behaviour vs. required/desired quality. In this line, the present work is aimed at developing a continuum 3D model, without predefined delamination surfaces, for the simulation of paperboard in-plane and out-of-plane responses during both creasing and folding, by employing the multipurpose FE code Abaqus, and assessing whether the basic characteristics of this responses can be reproduced with sufficient accuracy using features already present in the standard version of the code, without making recourse to customized user subroutines. This is highly desirable since considerable expertise on the use of the standard features in commercial software is already present in an industrial environment in most cases. This type of studies is often proposed in the

literature in view of its interest for the engineering community (see e.g. Girão 2016 [9], for a recent study on the simulation of delamination in composite materials using commercial finite element software).

One of the main issues in the setup of a computational model is the identification of the required constitutive parameters. In most cases, some of them have little impact on the analysis results and can therefore be assigned based on literature values, while others need be determined with higher accuracy. Furthermore, when the process to be simulated is complex, as in the creasing-folding sequence, it is possible that the importance of different parameters changes in passing from one process phase to the other. To the purpose of optimizing the identification procedure, a preliminary sensitivity analysis aimed at identifying critical parameters during specific process phases has been carried out. An optimization procedure has then been developed in an external code, based on a least squares formulation, iteratively invoking the FE code for material parameters identification. Several constitutive models available in the Abaqus material library have been considered for the matrix behavior and the corresponding parameters have been identified using this identification procedure. The industry oriented Abaqus models constructed in this way will be briefly referred to as "standard models".

For the critical comparative assessment of the different considered industry oriented models, reference has been made to results obtained using the model proposed in (Borgqvist et al 2015) [4] for creasing simulation and in (Borgqvist et al 2016) [5] for the simulation of folding (henceforth referred to as the "reference model"). It should be noted that the constitutive model presented in (Borgqvist et al 2015) [4] is an elastoplastic continuum model with hardening. No damage mechanisms are explicitly included to account for the loss of strength that is apparent in the late stage of delamination, for high folding angles. As shown in (Borgqvist et al. 2015) [4], the material response in the creasing process is well described by an elastoplastic model with a limited amount of hardening. The softening response in the folding process, is at least partially accounted for by the strong geometric effect brought in by the buckling of the compressed fibers, even though, as noted in (Borgqvist et al. 2016) [5], the ideal plastic assumption in the out-of-plane direction somehow overestimates the forces in the delaminated zone. The results obtained with the present model are however considered to be already useful for industrial applications and for the scope of the present paper. The objective of the paper is to test a continuum 3D finite element model based on standard features of a legacy code as Abaqus. The model developed in (Borgqvist et al. 2015) [4] and (Borgqvist et al. 2016) [5] is a continuum model, in contrast to the other hybrid models shortly discussed in the introduction, and it is implemented in an Abaqus User material. It is therefore ideal to be used as a reference for comparison purposes. The introduction of a softening model in Abaqus requires assigning a negative hardening together with a regularization scheme, to avoid mesh dependency. This could be achieved by tuning the softening parameters based on the element sizes in the localization zone. This aspect has however not been considered in the present work. Therefore, the model in (Borgqvist et al 2016) [5] has been used here also for the folding stage, in order to produce a consistent set of reference data spanning the whole process of creasing and folding.

In view of possible future applications to problems of industrial interest, all the analysis carried out in this work are 3D, but the problem to be simulated, i.e. creasing and folding of a paperboard strip, is very well approximated by a plane strain assumption. Therefore, a paperboard strip, one element thick in CD, has been used, assigning plane strain type of kinematic constraints to the model sides, thus mimicking by means of 3D elements a 2D model in the plane MD-ZD. In contrast, the reference analyses carried out with the reference model by Borgqvist et al (2015), implemented in an Abaqus User Material routine, were carried out using 2D elements.

The industry oriented approach proposed herein proves effective in qualitatively reproducing the main features of the creasing and folding processes, with acceptable quantitative accuracy. It allows understanding mechanical aspects of the phenomena taking place during creasing and folding, corroborating existing observations from the literature and highlighting some original peculiar aspects.

2. Paperboard three-dimensional constitutive model

2.1 Reference elastoplastic model

In (Borgqvist et al 2015) [4], the authors present a large strain continuum based, purely elastoplastic model (no damage) for paperboard possessing a high degree of anisotropy. The evolution of anisotropy is modeled by means of three structural tensors, defined as dyadic products of director vectors representing the preferred material directions, two of which associated to MD and CD, while the third to ZD. The in-plane director vectors deform as line segments, whereas the third deform as a normal vector. This is a key point in the kinematic formulation of the model, allowing for a decoupled in-plane and out-of-plane response in shearing.

Unlike it is customarily assumed in isotropic plasticity, a non-zero plastic spin is assumed, such that no plastic deformation occurs in the fibers stacking direction (initially the thickness direction) upon shearing. In this way, in the case of out-of-plane shearing, plastic deformation is due only to sliding between fiber layers.

The extreme material anisotropy is accounted for by defining a free energy density allowing for a decoupled in-plane and out-of-plane response, so that completely different parameters can be defined for the different deformation modes.

The plastic behavior is modelled using only one distortional hardening yield surface, inspired to the one proposed in (Xia et al., 2002) [25]. Linear hardening plasticity is assumed in ZD-compression, while a logarithmic expression is used for the hardening variables in the in-plane direction.

In (Borgqvist et al 2015) [4], the model has been shown to exhibit excellent accuracy for creasing simulations, while in (Borgqvist et al 2016) [5], it has also been used for folding simulations obtaining good results, even though an improvement is expected in the case that the possibility of developing damage is introduced into the model.

A large number of material properties need be specified for the complete definition of the model. However, the authors provide a clear identification strategy, trying to relate each individual parameter to its physical meaning, thus considerably reducing the complexity of the problem.

This material model, with parameters values suggested by the authors (see Tables A.1, A.2 and A.3 in Borgqvist et al 2015, [4]), has been used to generate reference data for paperboard creasing and folding. These data have then been used to tune and validate the finite element model, based on standard features, that will be discussed in the following sections.

2.2 Drucker-Prager constitutive models for paperboard matrix simulation

Following Borgqvist et al. (2015) [4], the three-dimensional paperboard behavior is modeled in this work as purely elastoplastic, with no damage.

The most natural choice to model continuum elastoplastic anisotropic behavior is the anisotropic-elastoplastic Hill model. Hill plasticity model has also been used in Beex and Peerlings (2009) [2] and in Huang et al. (2014) [14], though limited to modeling the in-plane behavior, the weaker out-of-plane behavior being accounted for by cohesive interfaces. Other more suitable anisotropic yield criteria, such as the Tsai-Wu criterion adopted e.g. in Harrysson and Ristinmaa (2008) [11], accounting for different strength in tension and compression, are not available in Abaqus [1] as fully three-dimensional elastoplastic material models and therefore cannot be used in the present study.

Positive features of Hill's model are: it allows for different yield stresses in different material directions leading to an anisotropic behavior in the plastic range; only few material parameters are required to define

the behavior of the model; Hill plasticity is suitable for both implicit and explicit analyses in several FE codes, including Abaqus. One of the main limitations of Hill plasticity model is that it accounts only for symmetric behavior in tension-compression. This is not suited to model the through-the-thickness paperboard strength that is much higher in compression than in tension. Another problem is the extremely high difference between out-of-plane and in-plane strength. As a consequence, for realistic material parameters the Hill yield surface turns out to have a very distorted geometry, difficult to treat computationally. These limitations suggest to undertake a different approach, whereby the higher material performance in MD-CD is reproduced by using a suitable reinforcement in those directions. Paperboard is hence modeled as a composite material where the matrix has non-symmetric, but otherwise isotropic elastoplastic properties, typical of the ZD behavior, and is modeled using solid elements, while the stronger in-plane MD and CD behaviors, are reproduced using suitable reinforcements embedded into the solid matrix.

The isotropic, plastically unsymmetrical Drucker-Prager (DP) (Drucker and Prager, 1952; Ottosen and Ristinmaa, 2005) [6] [23] continuum model is a candidate for reproducing the matrix isotropic ZD behavior, weaker in tension than in compression. The selected DP model is also usually available in the material libraries of the main multipurpose finite element codes, including Abaqus [1]. Several extensions and modifications of the DP model have been proposed in the literature (see e.g. Ottosen and Ristinmaa 2005 [23]), as shown in Figure 3.

The yield surface of the DP yield criterion, as it is implemented in Abaqus, is defined as follow:

$$F_s = t - p\tan\beta - d \tag{1}$$

where p is the hydrostatic stress, β the material friction angle, d the cohesion and t is defined as

$$t = \frac{1}{2}q\left[1 + \frac{1}{K} - \left(1 + \frac{1}{K}\right)\left(\frac{r}{q}\right)^3\right] \tag{2}$$

where q is the von Mises stress, r is the third stress invariant and K is the form factor of the yield surface in the deviatoric plane (Figure 3d). When K=1, the effective stress t coincides with the Mises stress q. The material has two different yield limits in uniaxial tension (σ_{0t}) and compression (σ_{0c}) and cannot reach the plastic limit under a hydrostatic compressive stress state (Figure 3a). Dilatancy can also be defined through the friction angle φ: if $\beta = \varphi$ an associated flow rule for plastic strains is obtained.

The DP model (Figure 3a) requires only few parameters for its definition and is suitable for both implicit and explicit analysis within the Abaqus framework. Common extensions of the original model are: the Cap-Drucker-Prager model (CAP-DP, Figure 3b) and the exponent yield criterion, which will be here referred to as Cut-Off-Drucker-Prager model (CO-DP). The latter, in the more general exponent form, is shown in Figure 3c. The CAP-DP model, limits the elastic domain under states of hydrostatic compression, allowing for the simulation of compacting features; in contrast, the CO-DP model limits the material hydrostatic tensile strength.

The CAP yield surface has an elliptical shape with constant eccentricity in the meridional plane (in green in Figure 3b). The cap surface hardens or softens as a function of the volumetric inelastic strain. The cap yield surface is defined as follows:

$$F_c = \sqrt{[p - p_a]^2 + \left[\frac{Rt}{(1 + \alpha - \alpha/\cos\beta)}\right]^2} - R(d + p_a\tan\beta) = 0 \tag{3}$$

where R and α are parameters controlling the shape of the CAP, d is the shear limit at zero pressure and p_a (see Figure 3b) is defined as

$$p_a = \frac{p_b - Rd}{1 + R\tan\beta} \tag{4}$$

The transition surface F_t between the linear domain and the CAP (Figure 3b) is defined as:

$$F_t = \sqrt{\left[p - p_a\right]^2 + \left[t - \left(1 - \frac{\alpha}{\cos\beta}\right)\left(d + p_a\tan\beta\right)\right]^2} - \alpha\left(d + p_a\tan\beta\right) = 0 \tag{5}$$

It is worth noting that dilatancy cannot be prescribed when using the CAP option. In this case, non-associativity is assumed by default for the DP surface in the meridional plane for the DP and transition surfaces, in the direction defined by the gradient of the plastic potential

$$G_c = \sqrt{[p - p_a]^2 + \left[\frac{Rt}{(1 + \alpha - \alpha / \cos\beta)}\right]^2} = 0 \tag{6}$$

In contrast, associativity is assumed for the cap and transition surfaces. When the stress point is on the CAP limit surface, a compacting behavior is simulated by the model.

Hardening/softening post-yield behavior can be prescribed by defining the hydrostatic compression parameter p_b as a function of the volumetric plastic strain ε_v^p . A compacting process can be simulated adopting an exponential hardening of the type: $p_b = p_{b0}e^{\varepsilon_v^p}$, where p_{b0} is the yield limit in hydrostatic compression. The resulting hardening curve is shown in Figure 4.

The exponent form of the CO-DP model (Figure 3c) is defined as:

$$F = aq^b - p - p_t = 0 \tag{7}$$

where *a* and *b* are material parameters independent of plastic deformation and p_t defines the yield limit under hydrostatic tension. Hardening is defined based on experimental measurements of yield stress from tests in uniaxial compression σ_{0c} , tension σ_{0t} or shear *d* (*d* being the cohesion):

$$p_t = a\sigma_{0c}^b - \frac{\sigma_{0c}}{3}; \quad p_t = a\sigma_{0t}^b + \frac{\sigma_{0t}}{3}; \quad p_t = ad^b \tag{8}$$

Also in this case the plastic flow is non-associated, according to a plastic potential given by

$$G = \sqrt{\left(\in \sigma_0 \tan\varphi\right)^2 + q^2} - p\tan\varphi \tag{9}$$

where $\in$ is a parameter, set equal to 0.1 by default, and φ is the dilation angle measured in the *p*-*q* plane at high confining pressure. Further details on the non-associated flow rule, can be found in the Abaqus Theory Manual.

2.3 Embedded reinforcements for reproducing the laminated paperboard in-plane behavior

Most multipurpose commercial FE codes allow implementing embedded elements, such as rebars, within plane or solid elements. These techniques are useful in the numerical simulations of composites and of reinforcements in concrete and soils. For this purposes, it is in general also possible to embed membranes and shell elements into a solid continuum. An alternative to the embedding approach is the overlapping

technique for FE meshes, successfully employed for reproducing global behavior of structures and components (see e.g. Gracia et al. 2010 [10]).

Within this framework, the paperboard in-plane behavior can be simulated by embedding layers of elements (with MD-CD properties) into the solid matrix (with ZD properties). The resulting model is a non-homogeneous, anisotropic continuum, intended to reproduce the highly anisotropic nature of the laminated structure. Either membrane or shell elements have been used as reinforcements. Even though other choices are allowed by the used software, embedded elements have been placed in MD-CD planes in such a way that they share the same nodes of the solid elements used for the matrix. In other words, the number of reinforcement layers depends on the number of elements used in the mesh in ZD. In the case of shell elements, rotational degrees of freedom are defined at these nodes in addition to the shared translational ones.

The paperboard in-plane behavior is slightly non-symmetric in tension/compression and this should be reflected by the reinforcement behavior in MD and CD. A user defined routine has been used to model the non-symmetric elastoplastic uniaxial reinforcement behavior. However, since in the applications this has been observed to produce only a negligible improvement in terms of accuracy, a standard isotropic von Mises elastoplastic symmetric model has been used for the reinforcements to simulate the in-plane paperboard response. Since only a relatively mild anisotropy is exhibited in the MD-CD plane, there would be no problem to use for the reinforcement an anisotropic Hill plasticity model instead of the considered isotropic Mises plasticity. However, only 2D applications are considered in this paper and the MD-CD anisotropy has been observed to play a negligible role on the final results. Therefore, isotropic plasticity has been assumed for the reinforcements. In practical 3D applications, e.g. with rotation creasing, MD-CD anisotropy could play a significant role and should be included in the model.

3. Creasing and folding simplified setups and finite element models

Creasing and folding, as they are carried out in the production line, are very complex processes. To investigate in detail the effect of various material and geometrical parameters and for the validation of the simulation models, simplified setups are usually considered. The simplified creasing setup (Figure 5) described in Nygards et al. (2009) [20] and later considered in Borgqvist et al. (2015) [4] has been used here to validate the proposed finite element model for the simulation of the creasing process. The simplified setup of the type described in Giampieri et al. (2011) [8] (Figure 6) has been adopted for the folding phase.

The creasing setup is shown in Figure 5. It consists of a male ruler, with a width b = 0.94 mm a height of 0.9 mm, and of a female groove, with a width W = 1.7 mm and a depth d = 0.8 mm. The paperboard is 80 mm long, 38 mm wide and 0.386 mm thick. The paperboard is pre-tensioned and clamped before creasing. The creasing process is carried out in the plane MD-ZD and consists of the following phases.

(i) A displacement is imposed at the paperboard ends to obtain the desired in-plane pre-tension. The applied pre-tension is recorded by a load cell placed at one of the paperboard extremities. The initial elongation is maintained throughout the creasing process to mimic the web tension occurring in production conditions.
(ii) The male ruler is lowered until it gets in contact with the paperboard.
(iii) The creasing process starts by pressing the paperboard into the female groove.
(iv) After the prescribed indentation depth is reached, the male ruler is lifted and the paperboard is unloaded.

During the indentation phase, extensive shear plastic deformation and damage are induced through the board thickness, producing a local weakening intended to facilitate the subsequent folding.

The folding setup is schematically shown in Figure 6. The paperboard is clamped at one end (right end in Figure 6) with a pressure of 0.2 MPa. The clamping terminates in correspondence of the beginning of the previously creased region. The out-of-plane deflection is contrasted by a load cell placed on the other side of the board. The load cell is placed at a distance of 10 mm from the end of the clamp. The clamp is rotated, forcing the board to fold around the creased region, and the imposed rotation and reaction at the load cell are recorded.

During folding, the reduced transverse cohesion between paperboard layers, as the result of shear-induced damage during creasing, allows delamination in thickness direction and buckling of the compressed layers (upper layers in Figure 6), releasing the tensile stress in the stretched layers on the other side (lower layers in Figure 6). In this way, creasing helps the folding process, preventing the possible occurrence of cracking on the stretched side.

The finite element models for the simulation of creasing and folding developed at Lund University (Borgqvist et al., 2015 [4] and Borgqvist et al., 2016 [5]) within the finite element code Abaqus have been kindly made available for comparison purposes in the present study. These models take advantage of the dominant two-dimensional nature of the problem and simulate creasing and folding using a mesh of plane strain 4-node isoparametric elements in the MD-ZD plane and an implicit non-linear dynamics approach. The male ruler used for creasing is lowered at a speed of 0.7 mm/sec, while a rotation of 0.08 rad/sec is imposed to the clamps in the case of folding.

Unlike the reference model, the finite element model developed in this research makes use of hexahedral 8-nodes isoparametric elements. This choice is motivated by the possibility offered by hexahedral solid elements in Abaqus to embed into the mesh a wider selection of element types (such as trusses, beams, shells, membranes) possibly allowing to explicitly take into account the material anisotropy in MD-CD. To allow for a more effective comparison with the results of the reference model, kinematic constraints corresponding to a plane strain idealization have been applied. A strip of material one element thick in CD, with lateral constraints preventing displacements in CD has been considered.

The simulation has been performed in an implicit dynamics framework by implementing a sequence of steps. The steps for the creasing phase are precisely those from (i) to (iv) previously listed. For the folding phase, the following steps have been implemented:

(v) The axial tension is eliminated by removing the axial restraints from the paperboard.
(vi) The paperboard is clamped at the right side, while the load cell is moved until it gets in contact with the paperboard on the left side of the mesh.
(vii) The folding process is started by rotating the clamp around the point marked in Figure 6, from 0° to 90°.
(viii) The clamp is rotated back to 0°.

Different values of the friction coefficient μ between the paperboard and the rigid tools have been used during creasing and folding in the FE models. For the female tool-paperboard and the clamping tool-paperboard interactions $\mu = 0.15$ has been adopted, for the load cell-paperboard interaction $\mu = 0.1$, while for the male tool-paperboard interaction $\mu = 0$ (no friction) has been used. Such values, withstanding to real conditions, has been consistently used for both the reference model and the one herein developed. Penalty exponential functions have been implemented for normal contact between the FE meshes and the analytical surfaces of the rigid tools.

The mesh for the standard model consists of 19 layers of solid elements in the paperboard thickness (ZD) and it is refined around the contact male, female and load cell tools. The mesh used for the reference model is a 2D mesh of 4-node, plane-strain elements in the MD-ZD plane, based on the same 19 layers, with identical node positions and number of elements, and homogeneous material. The finite element model, including

the tools rigid surfaces, is shown in Figure 7. The same mesh has been used for the simulation of creasing and folding. To simulate the highly different material properties between in-plane and thickness directions, 20 layers of reinforcements have been embedded in the in-plane directions, in correspondence of the element nodes. Membrane elements have been used in a first instance to model the reinforcement layers.

4. Creasing simulations: optimization procedure for parameters identification

Preliminary sensitivity analyses have shown that the constitutive parameters, in particular those defining the matrix behavior, but also those associated to the membrane behavior of the reinforcements, are more important in defining the paperboard response during creasing compared with the final folding process, which is mainly driven by nonlinear geometric effects. In particular, the matrix behavior plays a more important role in the initial part of creasing, when the plastic region starts to develop in the paperboard between the male and female tools, while the reinforcement properties are determinant in the later stages of creasing, when the combined action of the axial restraint and of the deep male tool displacement produce a significant reinforcement elongation.

These observations suggest that elastoplastic constitutive parameters should be identified during creasing. To this purpose, a “shallow” creasing (low indentation depth) is considered first, focusing the investigation on the constitutive properties characterizing the elastic-plastic transition in the matrix occurring at the beginning of the creasing process. The geometric effects (in-plane elongation due to transverse deflection) are in this case small and, therefore, the effect of the in-plane reinforcement on the transversal paperboard response is also very small. In later stages of creasing (deep creasing), the process is only mildly nonlinear, the main role being played by the reinforcements. Subsequently, deep creasing and folding conditions will be considered for the identification of the reinforcement properties.

4.1 Parameter identification procedure

An optimization procedure has been developed to identify the constitutive parameters during the creasing stage. The standard isotropic Drucker-Prager with cap (CAP-DP), for the matrix, and Mises, for the reinforcement layers, plasticity models have been initially used. For both models, a hardening behavior has been assumed, with no damage. These models require only a limited number of parameters. Furthermore, since matrix and reinforcement play specialized roles in determining the paperboard response, it is possible to understand the effect of the different parameters on the overall behavior.

The adopted identification strategy is based on an optimization algorithm, implemented in Matlab (2013) [18], whereby the optimal value of the sought parameters is obtained minimizing the discrepancy between the output of the Abaqus finite model obtained with the materials laws here adopted and with the one proposed in the reference model of Borgqvist et al. (2015) [4]. In other words, the results obtained with this latter model are used as a replacement for experimental data.

To the purpose of implementing the optimization iterative sequence, a Matlab procedure has been developed capable to invoke Abaqus at each iteration. The procedure is able to modify the Abaqus input file, to launch repeated analyses and to extract the required results from the Abaqus output file. Results of the FE model applications can be compared with the target curves obtained using the reference constitutive model. In this way, the procedure for parameters optimization is fully automatized.

The used optimization algorithm, available in Matlab, is the Trust Region-Reflective Least Square Optimization Method that allows to solve the optimization problem

$$\min_{x}\left\{ f(\mathbf{x}) = \sum_{s\in N}\left[g_{computed}(s,\mathbf{x}) - g_{target}(s)\right]^{2} \right\} \tag{10}$$

where **x** is the normalized vector of material parameters to be identified, $f(\mathbf{x})$ is the objective function to be minimized, termed *fitness function*, defined as the sum of squared discrepancies at N control points s between the computed analysis output $g_{computed}(s,\mathbf{x})$ and the target reference curve $g_{target}(s)$ for the current values of the material parameters **x**. The optimization procedure takes the vector **x** as input and defines a tentative variation $\Delta\mathbf{x}$ of the parameters vector. The procedure then automatically updates the FE input file with the new set of parameters ($\mathbf{x}+\Delta\mathbf{x}$) and runs a new analysis, generating a new curve $g_{computed}(s,\mathbf{x}+\Delta\mathbf{x})$. A Python script access the Abaqus results database and produces the required output. Finally, the output file is read by the Matlab procedure to extract the data necessary to compute the discrepancy function. At each iteration, the algorithm updates the current value of **x** to $\mathbf{x}+\Delta\mathbf{x}$, under the condition that $f(\mathbf{x}+\Delta\mathbf{x})<f(\mathbf{x})$. If for the selected trial value of $\Delta\mathbf{x}$ this condition is not satisfied, the parameters vector is not updated and a new tentative $\Delta\mathbf{x}$ is selected. The iteration sequence stops when $\Delta\mathbf{x}$ becomes sufficiently small, according to a predefined tolerance. The corresponding set of parameters is assumed as the optimal set to be considered. The problem is highly non-convex and multiple local minima are always to be expected, so that the optimal set in in general not unique.

Figure 8 shows the flow diagram of the implemented procedure.

4.2 Optimal parameters identification in shallow creasing

Parameters for the CAP-DP model (Figure 3b), used for the matrix, have been identified first. The CAP-DP model has been taken into consideration for the following reasons: it allows to account for the effect of pressure on the shearing behavior and of the compacting properties of paperboard in ZD. Thanks to the cap, it allows to relax the constraint on the plastic strain direction in the highly compressed region between the male and female tools, reducing the stiffness and enhancing convergence in the implicit dynamics procedure. In view of the highly non-convex nature of the fitness function, the optimization has been guided by selecting only two parameters to be identified, while the others have been assigned values taken from the literature or have been expressed as functions of the parameters to be identified. The choice of parameters to be used is essentially heuristic. Few attempts have been made with different pairs and the sensitivity of the output on these parameters has been assessed. The parameters producing the highest sensitivity have been selected. No rigorous strategy behind the selection of parameters to be used in the optimization is available at the moment.

The elastic limit in compression σ_{0c} and the elastic modulus in ZD E_{ZD} have been selected as search parameters. Other choices are also possible, but these parameters seem to be more critical in this early stage of creasing. Their starting values (σ_{0c} = 4 MPa and E = 130 MPa) have been prescribed based on literature data (Borgqvist et al. 2015 [4], Nygårds et al. 2009 [20]). The hardening parameters α and R, required to define the CAP surface (see eq. (3)), have been set to α = 0.025 and R = 3.8. The pressure p_b and the elastic limit in tension σ_{0t} have been defined as functions of the elastic limit in compression (p_b =10 σ_{0c}, σ_{0t} = 0.4 σ_{0c}). Isotropic membrane elements have been used as reinforcements in in-plane direction, thus neglecting the MD-CD difference, with von Mises elastoplastic properties taken from the literature and equal to the ones in MD (E_{MD} = 6611 MPa, ν = 0, yield limit σ_0 = 16.5 MPa, with isotropic hardening defined by pairs of values σ_h-ε_{eq}^{p} = 16.5-0.0; 44.0-0.01; 66.0-0.07; 98.0-1.0). The remaining used elastic parameters are: elastic modulus for the isotropic matrix taken equal to the one in ZD, ν_{ZD}=0, density ρ = 750x10^{-09} kg/mm^3.

Figure 9 shows the results of the iterative optimization (optimal parameters values σ_{0c} = 3.52 MPa and E_{ZD} = 115 MPa). It consisted of 15 iterations, a lower bound on the size of a step, meaning the norm of $\left\|\mathbf{x}^{n+1}-\mathbf{x}^{n}\right\|=0.001$, n being the iteration number, and a lower bound on the change in the value of the objective function during a step $\left|f(\mathbf{x}^{n+1})-f(\mathbf{x}^{n})\right|=0.001$. To improve the optimization results, a refinement

of the *N* evaluation points up to 230 has been used in the optimization process. The force applied to the male tool is plotted versus the male displacement (negative values, from right to left). Only the initial part of the creasing process, corresponding to a maximum indentation of 0.2 mm (shallow creasing), where plasticity develops and spreads through the thickness in the sheared region between the male and female tools, has been considered for the identification, since this is the part of the process where the plastic parameters play a more important role. The red line represents the target curve (obtained using the model in Borgqvist et al., 2015 [4]) and the black ones the trial curves obtained at each iteration. The blue dashed line has been obtained with the initial set of optimization parameters, while the continuous blue line is the one obtained with the optimal identified set. The optimal value of parameters is identified as the one leading to the minimum discrepancy between the target and trial curves.

Figure 10 shows the contour plots of effective plastic strains at the same level of creasing, obtained with the reference model and with the standard model here considered. The target reference model shows a slightly more extended plastic region, though with a higher value of plastic strains.
The qualitative pattern of effective plastic strain is similar in the CAP-DP and reference models (Figure 10). The optimization process in Figure 9 shows that the CAP-DP model leads to an early stiffness loss, due to plasticity, for small indentation depth, and to an overly stiff behavior in the later stage of creasing.

4.3 CO-DP model in the paperboard matrix

The results of the previous section have shown how the compacting behavior accounted for by the cap of the CAP-DP model is not crucial in the paperboard response. In contrast, the roles of the shear paperboard response, determined by the linear DP limit surface and by the dilatant flow rule, with different responses under positive and negative pressures, and of the shape of the limit surface for positive hydrostatic stresses appear to be essential. The latter aspect is explicitly accounted for, with a coupling between shear stress and normal tensile stress in ZD, in the yield surface used in Borgqvist et al. (2015) [4] for the definition of the reference model. The coupling also implies that there will be dilatation in ZD when the material is sheared. All these features are included in the DP model with Cut-Off on the positive pressure side (CO-DP), present in the Abaqus material library (Figure 3c).
The results of a preliminary parametric study are shown in Figure 11, where the CO-DP model has been employed. Parameter *a* has been defined from the first of equations (8) considering different values of the exponent *b* and of the dilatation angle φ, as shown in Figure 11a. The other parameters p_t, σ_{0c} have been taken equal to 0.1 MPa and 1.0, 2.0, 3.0 MPa, respectively. A perfectly plastic matrix response has been considered, with the same reinforcement properties used for the analyses in Figure 9. The penetration depth of the male ruler is the same as in the previous example (shallow creasing).

The positive effect of the elastic limit in tension and the role of the exponent *b* are elucidated in Figure 11a, where different values of the compression strength σ_{0c} and of dilatancy angle have been considered. Dilatancy seems to have only a minor effect on the global response during the creasing process, while the effect of *b* and σ_{0c} is more evident. The variation of the CO-DP domain in the meridional plane for different values of the exponent *b* and of the compression strength σ_{0c} is shown in Figure 11b: *b* determines the sharpness of the transition between the tension cut-off and the frictional part of the limit surface, while increasing the elastic limit in compression has the effect to amplify the elastic domain.

In conclusion, the CO-DP model provides more accurate results in reproducing the paperboard behavior during creasing. A satisfactory matching with the target results is achieved, as shown in Figure 12, for both the transversal and axial global responses during creasing. The used material parameters are: density ρ=750x10^{-09} kg/mm^3; matrix elastic moduli E_{ZD}=87 MPa, ν_{ZD}=0; reinforcement elastic moduli E_{MD}=6611 MPa, ν_{MD}=0; matrix plasticity parameters *a*=1.6646x10^{11}, *b*=20, σ_{0c} =3.52 MPa, φ=30°, p_t=0.1 MPa, perfect

plasticity, reinforcement yield limit σ_0=16.5 MPa; reinforcement hardening defined on the basis of pairs σ_h-ε_{eq}^{p} = 16.5-0.0; 44.0-0.01; 66.0-0.07; 98.0-1.0.

The identification procedure has been based on the optimal set of parameters defined in the previous section, with the same tolerance. The values φ=30° and p_t=0.1 MPa have been assigned based on physical considerations. As for the CAP-DP case, the elastic modulus in ZD E_{ZD} and the elastic limit in compression σ_{0c} have been selected as search parameters. A smaller number of iterations (8 iterations) than the one required in the identification of the previous section, has been used to identify the optimal parameters. This is reasonably due to the fact that in this case the initial set of parameters was the result of a previous optimization, and therefore probably closer to the optimal solution.

5. Extension to deep creasing

In section 4.2, only shallow creasing (0.2 mm male tool penetration) was considered for identification of the elastoplastic CO-DP matrix parameters. The simulation of deeper creasing (0.58 mm male tool penetration) is now considered to validate the developed Abaqus model. As previously pointed out, the reinforcement properties have a limited impact on the results in shallow creasing and therefore need be identified ex-novo for the case of deep creasing. The optimal parameters for the shallow creasing simulation turn out to be not optimal for the deep creasing case. The ZD elastic modulus and the elastic limit in compression have been identified first, assuming a value b = 10 of the exponent in (7), obtaining the values $E_{ZD} = 78$ MPa, $\sigma_{0c} = 5.5$ MPa. A friction angle φ = 10° has been identified by a parametric study, as in Figure 11a. The least-square optimization procedure discussed in section 4 has then been used to identify the elastic limit and the hardening parameters of the Mises plasticity model adopted for the membrane elements used as reinforcements in MD-CD. All other parameters have been taken identical to those used for the simulation in Figure 12. Figure 13 depicts the optimized hardening curve of equation $\sigma_h = \omega \varepsilon_p^{\frac{1}{\mu}} + \sigma_0$, used for the Mises plasticity model of the reinforcements, where ω μ and σ_0 are parameters to be identified. Their values in Figure 13 are 5100 MPa, 2 and 35 MPa, respectively. Ten iterations have been necessary for this identification.

The results of the simulation are shown in Figure 14 and Figure 15, with a comparison against the corresponding results obtained with the reference model. From Figure 14b, a good agreement is observed between the two models in terms of transverse response. The axial force developed in the in-plane directions at large creasing depth is however significantly different in the two cases. This discrepancy was not observed in the shallow creasing test, since in this case the geometric effect is negligible. Attempts to reduce the discrepancy in the in-plane direction, while preserving the good accuracy in the transverse direction, have not been successful. This may be due to the special treatment of shear inter-layer plastic deformations allowed for by the reference model (see Borgqvist, 2015 [4] for details), which cannot be replicated by the simple Abaqus model based on standard features here considered. Altogether, despite the simplicity of the model, the quality of the simulation appears to be comparable to that of most of the other, more complex models available in the literature (see e.g. Huang et al., 2014 [14], Beex and Peerlings, 2009 [2]).

The contour plot of the equivalent plastic strains is shown in Figure 15a at the maximum indentation depth. The deformed shape at real scale of the reinforcement membranes is shown Figure 15b. The contour plot of plastic strains obtained with the reference model is shown in Figure 15c.

6. Folding simulations

The Abaqus finite element model, optimized and validated for the creasing process in the previous sections, is now used for the simulation of the folding process, based on the simplified setup described in section 3 (Figure 6). As previously discussed, the main feature of the model is to account for the high anisotropy by

means of reinforcements in MD-CD. In the initial identification phase, the reinforcements have been modeled by means of membrane elements embedded within a matrix of 8-node solid elements, with properties determined based on the ZD behavior. The parameters identified in the previous section for the deep creasing simulation have been initially assumed. The simulation of folding has been carried out after simulating a creasing at a depth of 0.58 mm.

As shown in Figure 6, the folding is achieved by clamping the right part of the paperboard and by rotating it around a rotation center placed in the position marked by a cross in the same figure. A pressure of 0.05 MPa is applied to the clamps to firmly keep the right part of the paperboard in its position.

The deformed shape obtained for a folding angle of 90° is depicted in Figure 16a. If compared to the physical process in Figure 1b, it is evident that the model does not allow for a complete buckling of the compressed layers. The paperboard fibers in MD show a local bulging only, with very short wavelength, which is not sufficient to reproduce the global buckling of the compressed layers occurring in the physical process. This is mainly due to the lack of bending stiffness of the membrane elements used for the reinforcements in MD. Though membrane elements may appear to be the most natural choice for the modelling of the in-plane reinforcements, these results clearly show that, while producing satisfactory results in the creasing phase, they are not suitable for the folding phase.

To overcome the problem, the membrane elements have been replaced by shell elements (4-node, fully integrated, general-purpose, finite-strain shell element), endowed with a bending stiffness to be tuned on the basis of a simulation of the creasing process. Even though the reinforcements play a minor role in the creasing phase, the additional bending stiffness alters the results and makes a new parameter identification necessary. Figure 16b shows the final configuration obtained with embedded shells after a 90° folding. The different response is clearly visible: the use of shell elements for the reinforcement produces a well-defined bulging of the compressed parts, with very large out-of-plane plastic strains (represented in the figure by a large localized stretch of some element layers), promoted by the shear inelastic deformations produced in the preceding creasing phase. The shape of the deformed paperboard, closely resembles the one in the physical process (Figure 1b), with the buckling of the compressed layers and consequent delamination. The wavelength of the bulging is comparable to the one of the buckled configuration observable in Figure 1b.

6.1 Optimal parameters for creasing and folding

Using the optimization procedure described in section 4, a new parameter optimization has been carried out for the new model with in-plane reinforcements discretized by shell rather than membrane elements. Two set of parameters, set “A” and set “B” have been identified as detailed below. The two sets share the same parameters for the CO-DP matrix, whereas they have different values of elastic modulus, Mises yield stress and thickness for the reinforcements. The reason for considering two different sets rests in the difficulty of carrying out the optimization in the creasing phase only, since the bending stiffness of the reinforcements turns out to affect both phases. With the present functionality of the optimization tool, it is however impossible to perform an optimization over the complete creasing and folding sequence. The selected parameters sets are reported below.

Model “A”

CO-DP matrix: E_{ZD}= 78 MPa, ν_{ZD}=0, b=10, ρ=750x10^{-09} kg/mm^3, p_t=0.1 MPa, φ=10°, σ_{0c}=5.5 MPa, perfect plasticity, Rayleigh damping α=0.62, β=0.000158)

MISES shells: E_{MD}= 23798 MPa, ν_{MD}=0, reinforcement hardening defined on the basis of pairs σ_h-ε^p_{eq} = 35.0-0.0, 1180.0-0.05, 1650.0-0.1, 3660.0-0.5, 4600.0-0.8, 5100.0-1.0., thickness = 0 .0050789 mm

Model “B”

CO-DP matrix: E_{ZD}= 78 MPa, ν_{ZD}=0, b=10, ρ=750x10^{-09} kg/mm^3, p_t=0.1 MPa, φ=10°, σ_{0c}=5.5 MPa, perfect plasticity, Rayleigh damping α=0.62, β=0.000158)

MISES shells: E_{MD}= 18306 MPa, ν_{MD}=0, reinforcement hardening defined on the basis of pairs σ_h-ε_{eq}^{p} = 44.0-0.0, 1470.0-0.05, 2070.0-0.1, 4575.0-0.5, 5775.0-0.8, 6452.0-1.0., thickness = 0.0066 mm

The obtained global responses in terms of axial and transversal creasing force-displacement diagrams and folding moment-clamp rotation diagrams are shown in Figure 17. The final deformed shapes at the end of the folding phase are shown in Figure 18. While for both sets a good qualitative agreement is obtained in all phases, set “B” gives a better accuracy in the creasing phase, whereas the model employing set “A” is more accurate in the folding phase.

6.2 Effects of boundary conditions

Comparing the deformed shape of the reference model in Figure 18a with the ones in Figure 18b and c, one can notice that the first exhibits and almost perfect symmetry, while the other two are clearly not symmetric. This difference, that does not compromise the overall good qualitative result, can be interpreted as due to the inhomogeneous nature of the developed finite element model, as the presence of the in-plane reinforcements increases the sensitivity of the model to the imposed boundary conditions.

To elucidate this aspect, additional finite element analyses have been carried out considering a paperboard with perfectly linear elastic properties (those of model “B” have been used) for both the solid matrix and the shell elements in the reinforcements. The same model, without the shell layers (i.e. where only the homogeneous solid matrix has been considered), has also been analyzed and compared to the previous one.

The loading and the boundary conditions are those of a self-equilibrated configuration (Figure 19a, self-equilibrated bending moments applied at the right side of the structure). Figure 19b depicts the von Mises effective stresses in the non-homogeneous paperboard, while Figure 19c in the homogeneous one. The embedded shell layers in the non-homogeneous model have the effect to propagate the disturbance on the right-side along a distance extending through a significant length of the mesh. On the contrary, as expected according to De Saint Venant principle, stresses in the homogeneous model, due the self-equilibrated external forces applied at the beam end, vanish at a distance comparable to the paperboard thickness.

The same test has been repeated using the complete elastoplastic parameters of set “B” obtaining the same type of response. The results are shown in Figure 20.

Based on these results, one can conclude that the in-plane reinforcements used to simulate the high anisotropy have the effect to increase the length of propagation of the boundary effects. This consideration can explain the lack of symmetry of the deformed configuration after folding, which can be observed only in the non-homogeneous model. The clamps on the right part of the paperboard and their rotation produce a non-symmetric stress distribution in the central part of the creased region, with the final effect of inducing a non-symmetric deformation during folding. This enhanced sensitivity to boundary conditions should be taken into account when using an approach of this type for the treatment of anisotropy.

6.3 Mesh dependence

The analyses in the previous subsections have shown that qualitatively good results, of potential usefulness for application in an industrial environment, can be obtained by suitably tuning a finite element model based on standard features available in a commercial finite element code. However, only simulations with highly

refined meshes of simplified test setups have been considered, whereas it would be of obvious interest to consider less refined models, applicable also for the simulation of real scale creasing and folding processes.

To investigate the performance of the proposed model when used with a coarse mesh, a mesh with only 6 layers of solid elements and 7 layers of shell reinforcements through the thickness (with a scale factor of 3.16 between the elements in the fine and coarse meshes) has been analyzed using the parameters of set "A". The thickness of the embedded shells has been scaled using the same scale factor of the solid elements. The complete set of adopted parameters is listed below.

Model "A" COARSE

CO-DP matrix: E_{ZD}= 78 MPa, v_{ZD}=0, b=10, ρ=750x10^{-09} kg/mm^3, p_t=0.1 MPa, φ=10°, σ_{0c}=5.5 MPa, perfect plasticity, Rayleigh damping α=0.62, β=0.000158)

MISES shells: E_{MD}= 23798 MPa, v_{MD}=0, reinforcement hardening defined on the basis of pairs σ_h-ε_{eq}^{p} = 35.0-0.0, 1180.0-0.05, 1650.0-0.1, 3660.0-0.5, 4600.0-0.8, 5100.0-1.0., thickness = 0 .01605 mm

The original fine and the new coarse meshes are shown in Figure 21.

The results of the analyses with the new coarse mesh are shown in Figure 22. These results show that the coarse mesh can be conveniently used for the simulation of the creasing process, since the obtained accuracy is almost comparable to the one obtained with the fine mesh. As expected, the coarser mesh leads to a significantly stiffer response in the later stage of folding, even though the qualitative behavior is still reproduced.

7. Conclusions

Paperboard creasing and folding are complex mechanical processes, highly nonlinear due to the strongly anisotropic elastoplastic material behavior and to the very large deformations involved. The capability to estimate a qualitative mechanical response of paperboard during these processes, such that the risk of cracks or other types of defects can be predicted, is of great importance in an industrial context and requires robust models that can converge also in the case of these complex loading scenarios. To this purpose, the possibility to carry out realistic and accurate simulations of paperboard creasing and folding developing a purely phenomenological model, aimed at capturing the overall paperboard response during creasing and folding and based on standard features present in a commercial finite element code, has been investigated. The use of standard features, on which a considerable expertise is in most cases already present in the industry, is also considered to be of great interest.

The results obtained with the developed finite element model have been validated by comparison with the results obtained with a recently proposed material model (termed "reference model"). The reference model in (Borgqvist et al. 2015) is very accurate and can be considered to represent the current state of the art for the simulation of paperboard behavior in creasing and folding. The two models have been used with the same data to simulate creasing and folding in simplified setups and the results have been critically compared.

Several different options have been considered for the definition of the model proposed in this work, trying to overcome the intrinsic difficulty of the extremely high anisotropy between the in-plane and thickness responses. The final adopted model consists of a non-homogeneous arrangement, with a homogenous matrix with ZD properties, discretized by means of hexahedral solid elements, and reinforcement layers of shell elements in the MD-CD planes embedded within the solid matrix. The matrix material has been modeled as an elastoplastic hardening material, with non-associated plastic flow, obeying the CO-DP model described in section 2.3. An optimization procedure has been implemented for identifying the material parameters in the creasing phase, by linking the finite element code to an external optimization routine, developed in Matlab, based on an ordinary least squares optimization method.

The proposed model has been able to effectively reproduce the main features of the target response, in both the creasing and subsequent folding phases, with good qualitative accuracy. Both the reference model and the model proposed in this work are able to reproduce the typical deformation patterns in the creasing and subsequent folding operations. In the folding phase, the global reduction of the folding moment is accounted for by the geometric effect promoting the bulging of the compressed fibers, mimicking the buckling of the compressed paperboard layers in the real process. The bulging on the compressed side is accompanied by extensive plastic strains in ZD, which limit the lateral confinement on the compressed fibers. While the deformed configuration reproduces well the physical process, as noted in (Borgqvist et al. 2016), the ideal plastic assumption in the out-of-plane direction somehow overestimates the forces in the delaminated zone. Despite this limited quantitative accuracy, the simplicity of the model, the small number of material parameters to be identified and the overall qualitative accuracy of the results make it attractive for applications in an industrial contest.

The deformed configuration produced by delamination of fiber layers in the physical process cannot be reproduced when embedding membrane elements, but when using shell elements, the overall pattern can be recovered, with very large out-of-plane plastic strains. Isotropic behavior has been assumed for the shell elements, thus neglecting the MD-CD anisotropy. This simplification has no effect in the 2D simulations considered in this work. MD-CD anisotropy could be however easily considered in the case of more realistic 3D applications. The model has been shown to be sufficiently accurate with coarse meshes for the simulation of creasing, whereas an overly stiff response is obtained in the folding phase. It has also been shown how the presence of the reinforcements introduces a spurious dependence of boundary conditions that should be carefully considered in practical applications.

Among others, the following positive aspects of the developed standard model are worth highlighting:

- it employs a very limited number of parameters that can be effectively identified by an optimization procedure;
- by separating the role of the solid matrix with ZD properties from the one of the reinforcement layers, the proposed model allows for effective interpretations of the response mechanisms involved in the creasing and folding processes, allowing for a better understanding of critical aspects of the paperboard response, potentially useful for improvements in new packaging solutions.

In summary, the following main conclusions can be drawn for the construction of a finite element model based on standard features available in a commercial code and for its applicability.

- Standard anisotropic continuum plasticity models, such as Hill's model, appear to be hardly usable due to the extremely high anisotropy (ZD vs. MD and CD). A composite model, with a matrix having ZD properties and in-plane reinforcements has proven to provide satisfactory results for industrial applications.
- Shell elements rather than membrane elements should be used for the reinforcement modeling, since membrane elements fail to correctly reproduce the paperboard behavior in the folding phase.
- The matrix and the reinforcement constitutive parameters should be identified based on the results of deep creasing tests.
- The bending part of the reinforcement constitutive parameters should be identified based on the results of folding tests.
- The proposed model does not seem to be able to reproduce with the same level of accuracy both the transverse and the in-plane behavior in the case of deep creasing.
- Though the proposed model is able to reproduce the qualitative paperboard response in the folding phase, an overly stiff response is obtained.
- A rather coarse mesh can be conveniently used for the simulation of the creasing process, though at the cost of a significantly stiffer response in the later stage of folding.

- The composite nature of the model makes it particularly sensitive to the boundary conditions. Their definition and effects need therefore to be carefully considered.

Altogether, with the limitations evidenced in the numerical tests discussed in this paper, the quantitative response is sufficiently accurate for applications in an industrial environment and the approach turns out to be of practical interest in the previously defined perspective to develop a simulation tool for the identification of a safe process parameter space for paperboard creasing and folding.

References

[1] Abaqus. Abaqus 6.14 Documentation, Dassault Systèmes 2014.

[2] Beex, L. A. A. and Peerlings, R. H. J. An experimental and computational study of laminated paperboard creasing and folding, International Journal of Solids and Structures **2009**; **46**, 4192-4207.

[3] Borgqvist, E., Lindström, T., Tryding, J., Wallin, M. & Ristinmaa, M. Distortional hardening plasticity model for paperboard, International Journal of Solids and Structures **2014**; **51**, 2411-2423.

[4] Borgqvist, E., Wallin, M., Ristinmaa, M., Tryding, J. An anisotropic in-plane and out-of-plane elastoplastic continuum model for paperboard, Composite Structure **2015**; **126**, 184–195.

[5] Borgqvist, E., Wallin, M., Tryding, J., Ristinmaa, M. & Tudisco, E. Localized deformation in compression and folding of paperboard, Packaging Technology and Science **2016**; **29**, 397-414.

[6] Drucker, D.C., Prager, W. Soil Mechanics and Plastic Analysis or Limit Design, Quarterly of Applied Mathematics **1952**; **10**, 157–165.

[7] Dunn, E., Micromechanisms of Paperboard Deformation, MSc thesis in Mechanical Engineering, M.I.T. 2000.

[8] Giampieri, A., Perego, U. and Borsari, R. A constitutive model for the mechanical response of the folding of creased paperboard, International Journal of Solids and Structures **2011**; **48**, 2275-2287.

[9] Girão C., A. Finite element guidelines for simulation of delamination dominated failures in composite materials validated by case studies, Archives of Computational Methods in Engineering **2016**; **23**, 363-388.

[10] Gracia, L.A., Liarte, E., Pelegay, J.L., Calvo, B. Finite element simulation of the hysteretic behavior of an industrial rubber. Application to design of rubber components, Finite Elements in Analysis and Design **2010**; **46 (4)**, 357-368.

[11] Harrysson, A., Ristinmaa, M. Large strain elastoplastic model of paper and corrugated board, International Journal of Solids and Structures **2008**; **45**, 3334-3352.

[12] Huang, H. and Nygårds, M. A simplified material model for finite element analysis of paperboard creasing. Nordic Pulp and Paper Research Journal. **2010**; **25,** 505-512.

[13] Huang H. and Nygårds M. Numerical and experimental investigation of paperboard folding. Nordic Pulp and Paper Research Journal, **2011**; **26**, 452-467.

[14] Huang, H., Hagman, A. and Nygårds, M. Quasi static analysis of creasing and folding for three paperboards, Mechanics of Materials **2014**; **69**, 11-34.

[15] Kulachenko, A., Uesaka, T. Direct simulations of fiber network deformation and failure, Mechanics of Materials **2012**; **51**, 1-14.

[16] Li, Y., Simon, J.-W. Reese, S., Experimental and numerical investigation of paperboard creasing, Proceedings in Applied Mathematics & Mechanics **2014**; **14**, 1, 589-590.

[17] Li Y, Stapleton SE, Simon JW, Reese S., Experimental and Numerical Study of Paperboard Interface Properties, Experimental Mechanics **2016**; 1-12, doi:10.1007/s11340-016-0184-8.

[18] Matlab. Matlab R2013b, The Mathworks 2013.

[19] Nagasawa, S., Fukuzawa, Y., Yamaguchi, T., Tsukatani, S., Katayama, I. Effect of crease depth and crease deviation on folding deformation characteristics of coated paperboard, Journal of Materials Processing Technology **2003**; **140 (1–3)**, 157–162.

[20]Nygårds, M., Just, M. and Tryding, J. Experimental and numerical studies of creasing of paperboard, International Journal of Solids and Structures **2009**; **46**, 2493-2505.

[21]Nygårds, M. Experimental techniques for characterization of elastic-plastic material properties in paperboard Nordic Pulp and Paper Research Journal **2008**; **23(4)**, 432-437.

[22]Ortiz, M. and Pandolfi, A., Finite-deformation irreversible cohesive elements for three-dimensional crack-propagation analysis, International Journal of Numerical Methods in Engineering **1999; 44**, 1267–1282.

[23]Ottosen, N.S., Ristinmaa, M. The Mechanics of Constitutive Modeling, Elsevier 2005. ISBN: 978-0-08-044606-6.

[24]Xia, Q., Mechanics of inelastic deformation and delamination in paperboard, PhD Thesis, Massachusetts Institute of Technology 2002.

[25]Xia, Q., Boyce, M. C. and Parks, D. M., A constitutive model for the anisotropic elastic–plastic deformation of paper and paperboard, International Journal of Solids and Structures **2002**; **39**, 4053-4071.

Published in: Packaging Technology and Science 2017, DOI: 10.1002/pts.2298

a) 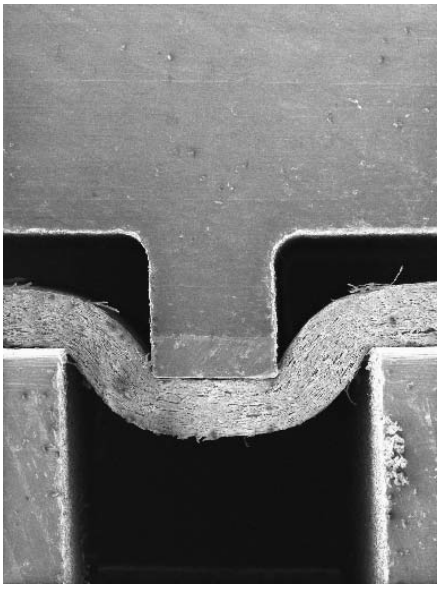 b) 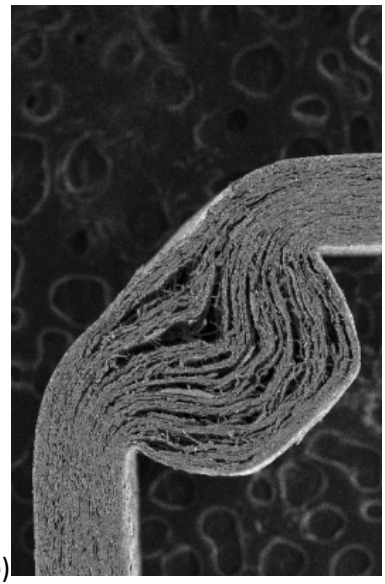

Figure 1 – Creasing process (a) (Dunn 2000[7]). Folding process (b) (Nagasawa et al. 2003 [19]).

Published in: Packaging Technology and Science 2017, DOI: 10.1002/pts.2298

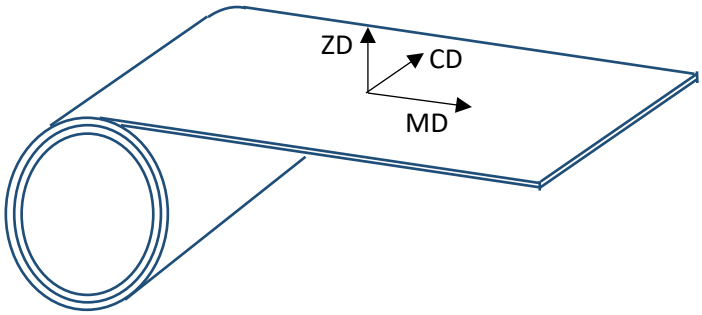

Figure 2 - Paperboard material preferential directions resulting from the manufacturing process: MD machine direction, CD cross direction and ZD thickness direction.

Published in: Packaging Technology and Science 2017, DOI: 10.1002/pts.2298

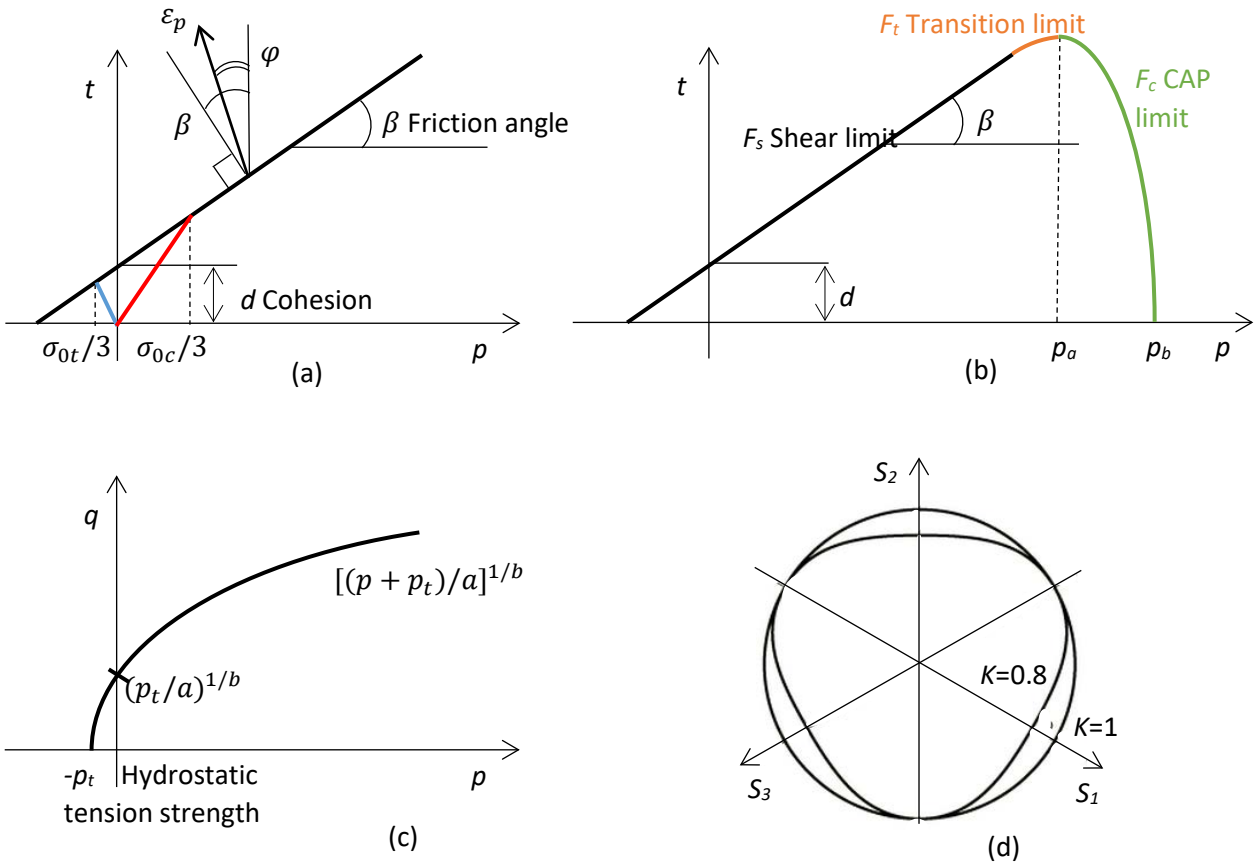

Figure 3 - DP (a), CAP-DP (b), CO-DP (c) models in the meridional (p-t) plane. DP model in the deviatoric plane. Dependence on K parameter (d).

Published in: Packaging Technology and Science 2017, DOI: 10.1002/pts.2298

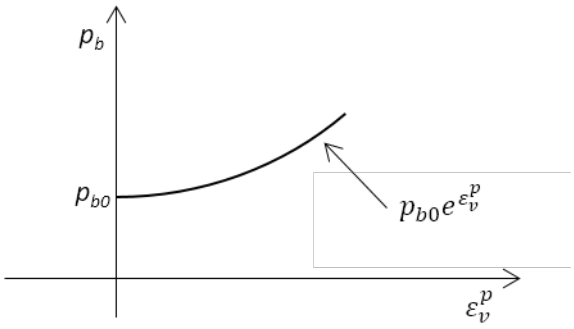

Figure 4 – Example of CAP hardening for paperboard compacting process.

Published in: Packaging Technology and Science 2017, DOI: 10.1002/pts.2298

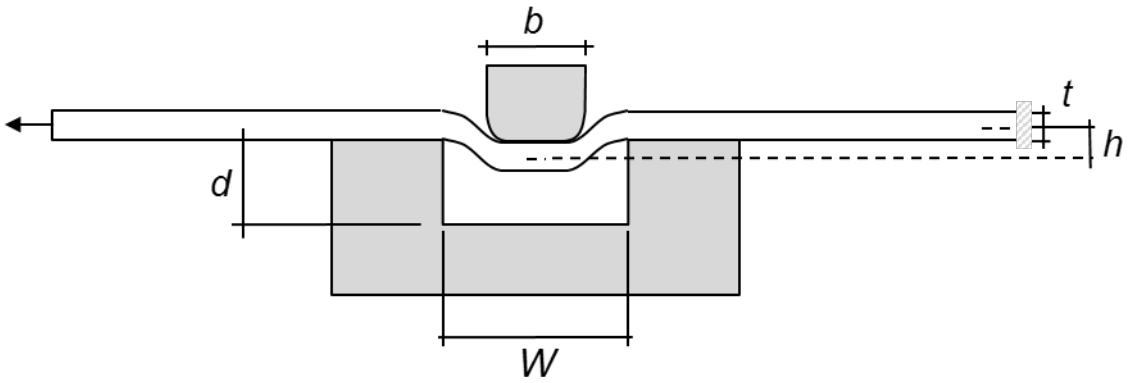

Figure 5 - Creasing test: experimental setup (a); detail of the finite element mesh (b).

Published in: Packaging Technology and Science 2017, DOI: 10.1002/pts.2298

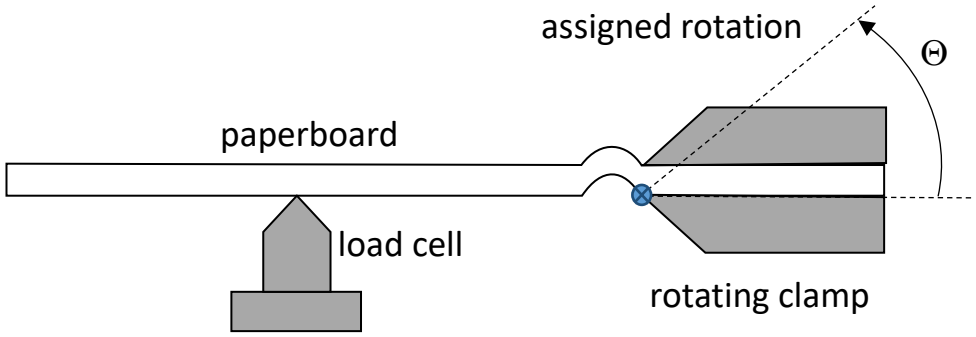

Figure 6 – Folding test. Experimental setup.

Published in: Packaging Technology and Science 2017, DOI: 10.1002/pts.2298

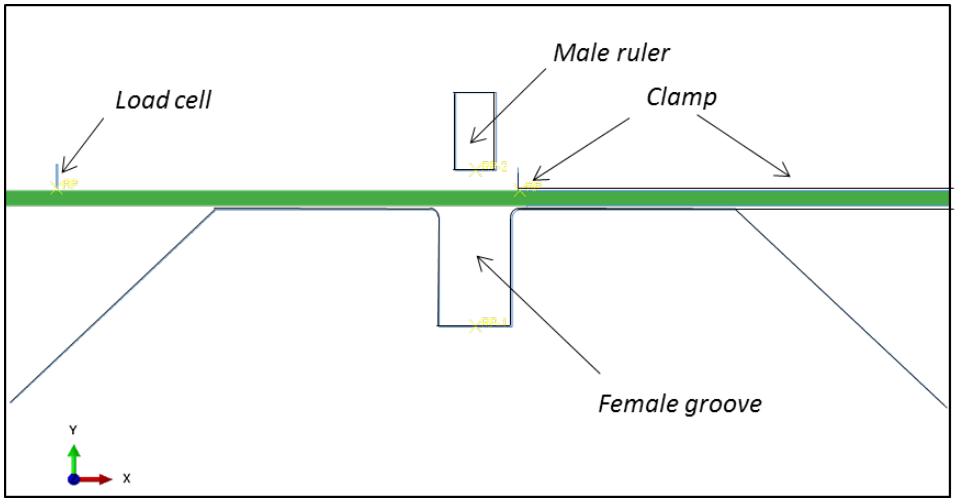

Figure 7 – Finite element model for creasing and folding.

Published in: Packaging Technology and Science 2017, DOI: 10.1002/pts.2298

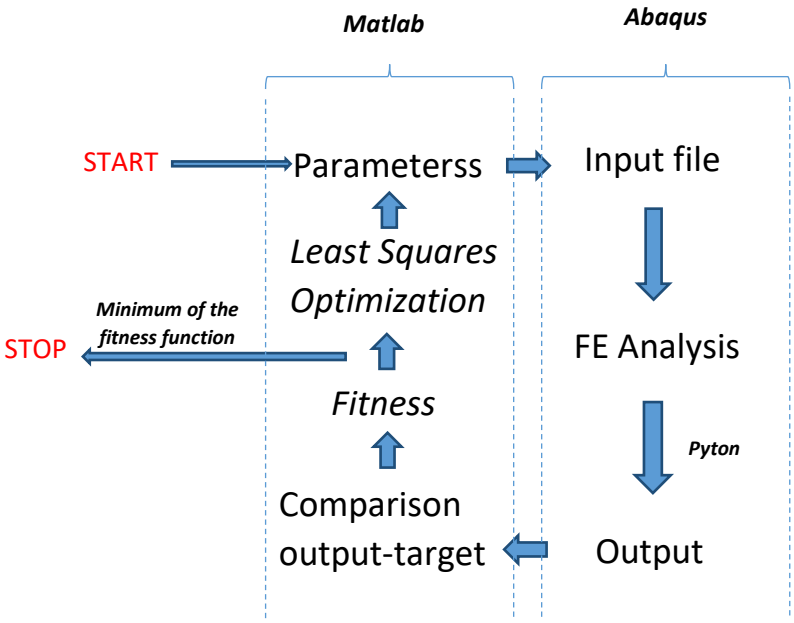

Figure 8 - Flow diagram of the optimization procedure.

Published in: Packaging Technology and Science 2017, DOI: 10.1002/pts.2298

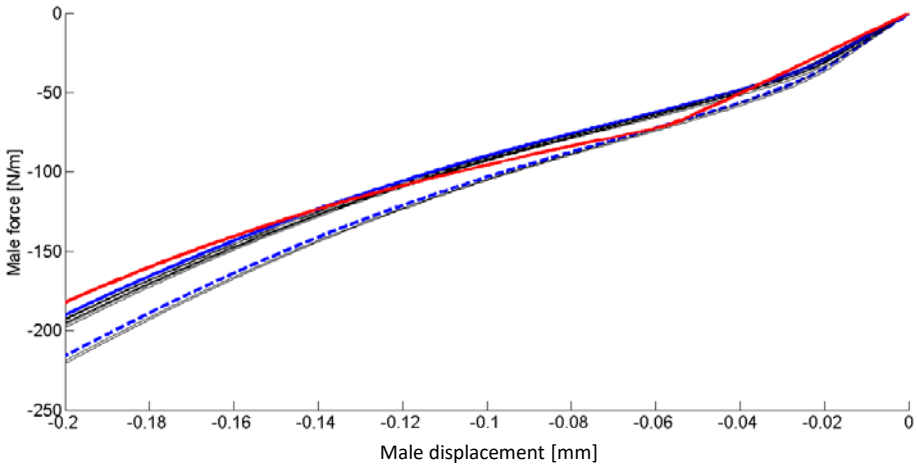

Figure 9 - Optimization procedure for parameters of CAP-DP model for matrix material. Creasing process (red curve – target reference model, black curves - iterations, blue solid curve - optimal parameter set, blue dashed curve – initial choice of parameters).

Published in: Packaging Technology and Science 2017, DOI: 10.1002/pts.2298

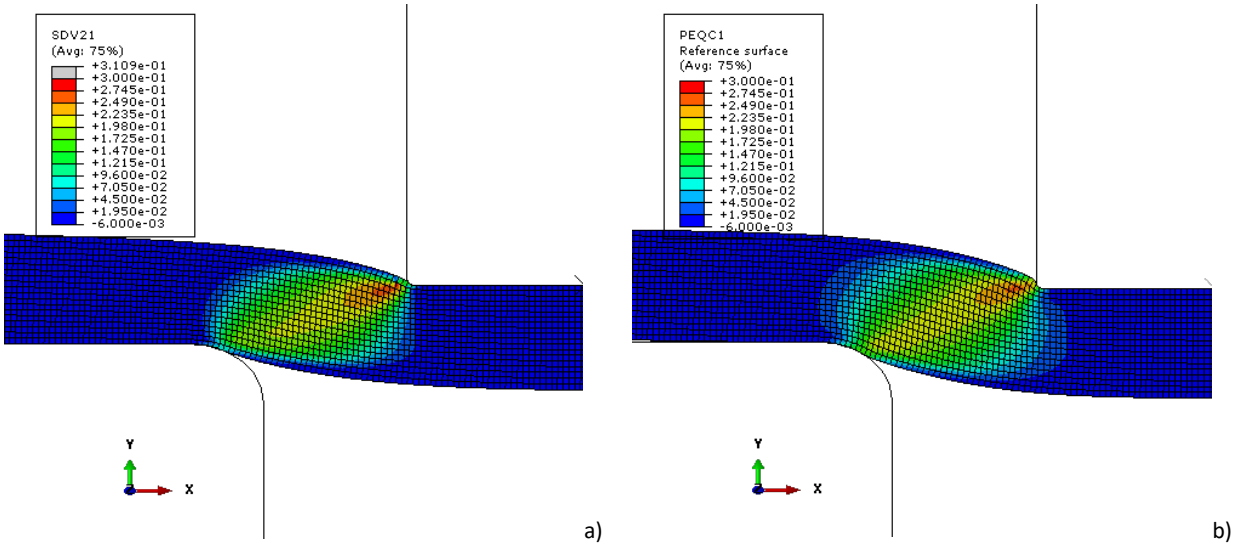

Figure 10 – Target reference model (effective plastic shear - a) and considered standard model (equivalent plastic strain linear CAP-DP limit surface) - b) on the same scale.

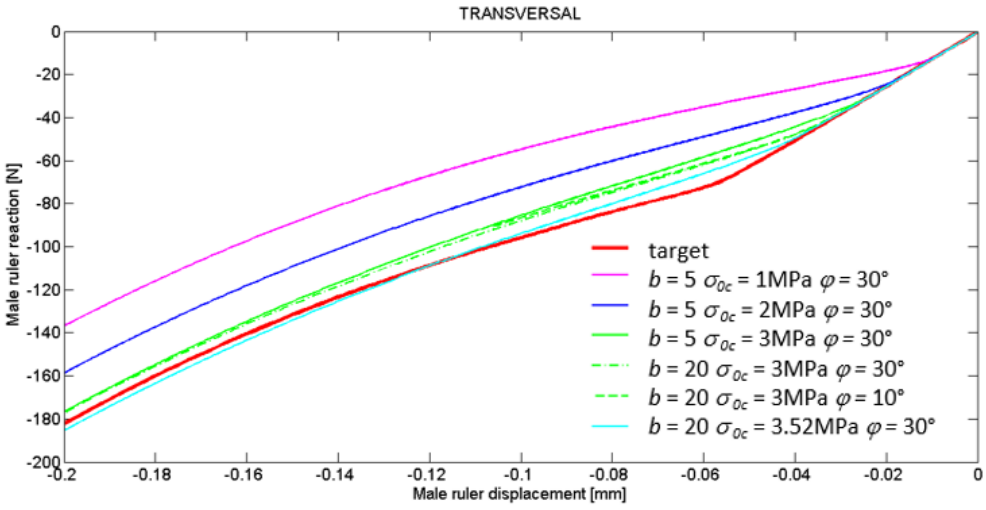

a)

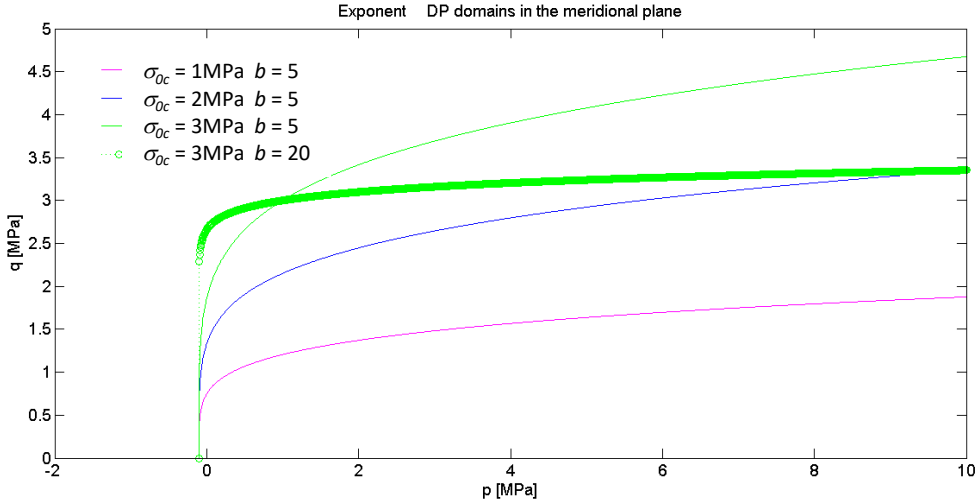

b)

Figure 11 - Parametric analysis (a) using the CO-DP model for the paperboard matrix in the creasing process (p_t=0.1 MPa); (b) CO-DP domains in the meridional plane.

Published in: Packaging Technology and Science 2017, DOI: 10.1002/pts.2298

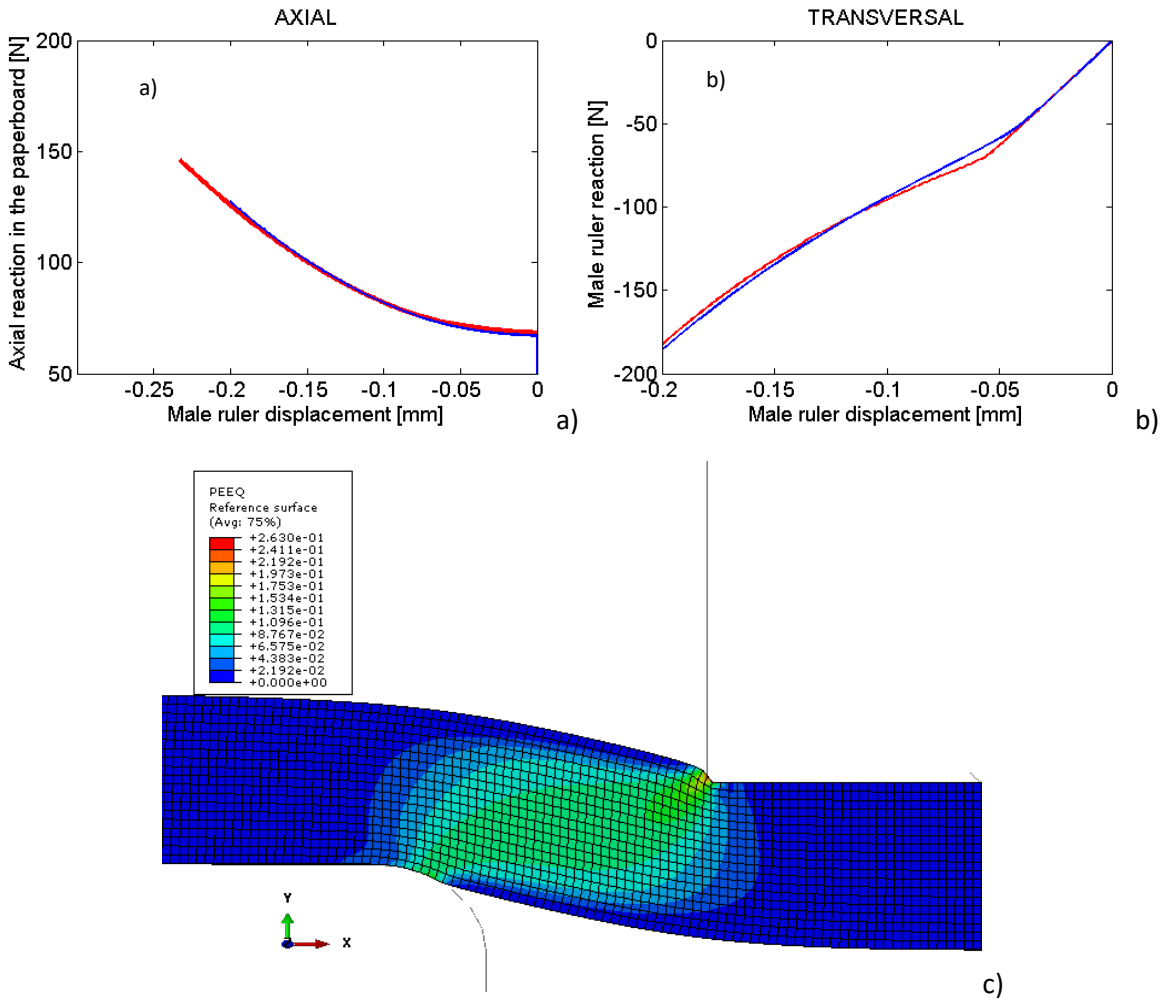

Figure 12 - Best matching simulation with the CO-DP model. (a) Axial response, (b) transversal response, (c) contour plot of equivalent plastic strain.

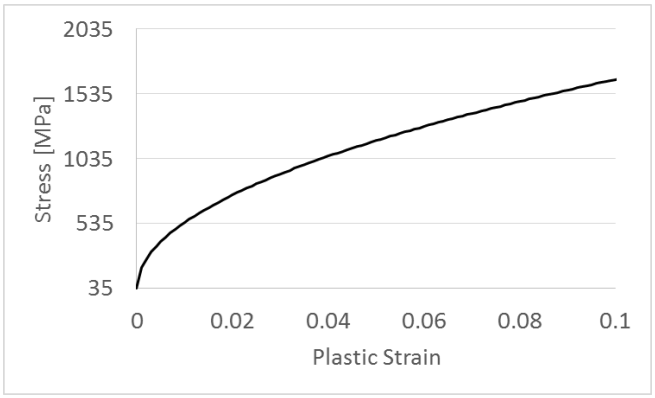

Figure 13 – Hardening law for reinforcement Mises plasticity model (with $\omega = 5100\ MPa,\ \mu = 2,\ \sigma_0 = 35\ MPa$).

Published in: Packaging Technology and Science 2017, DOI: 10.1002/pts.2298

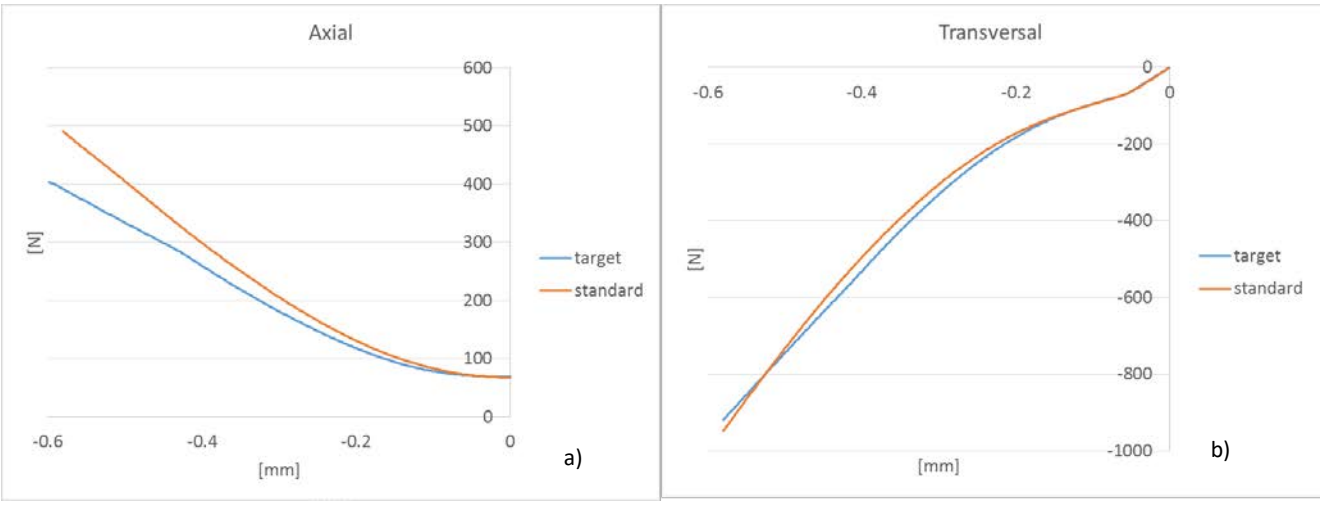

Figure 14 - Axial (a) and transversal (b) global responses of the target and the standard model (CO-DP matrix: E_{ZD}*= 78 MPa,* ν_{ZD}*=0,* b*=10,* ρ*=750x10^{-09} kg/mm^3,* p_t*=0.1 MPa,* φ*=10°,* σ_{0c}*=5.5 MPa, perfect plasticity. MISES reinforcements:* E_{MD}*= 6611 MPa,* ν_{MD}*=0,* σ_0*=35 MPa, hardening as in Figure 13, with* $\omega = 5100\ MPa,\ \mu = 2,\ \sigma_0 = 35\ MPa$ *).*

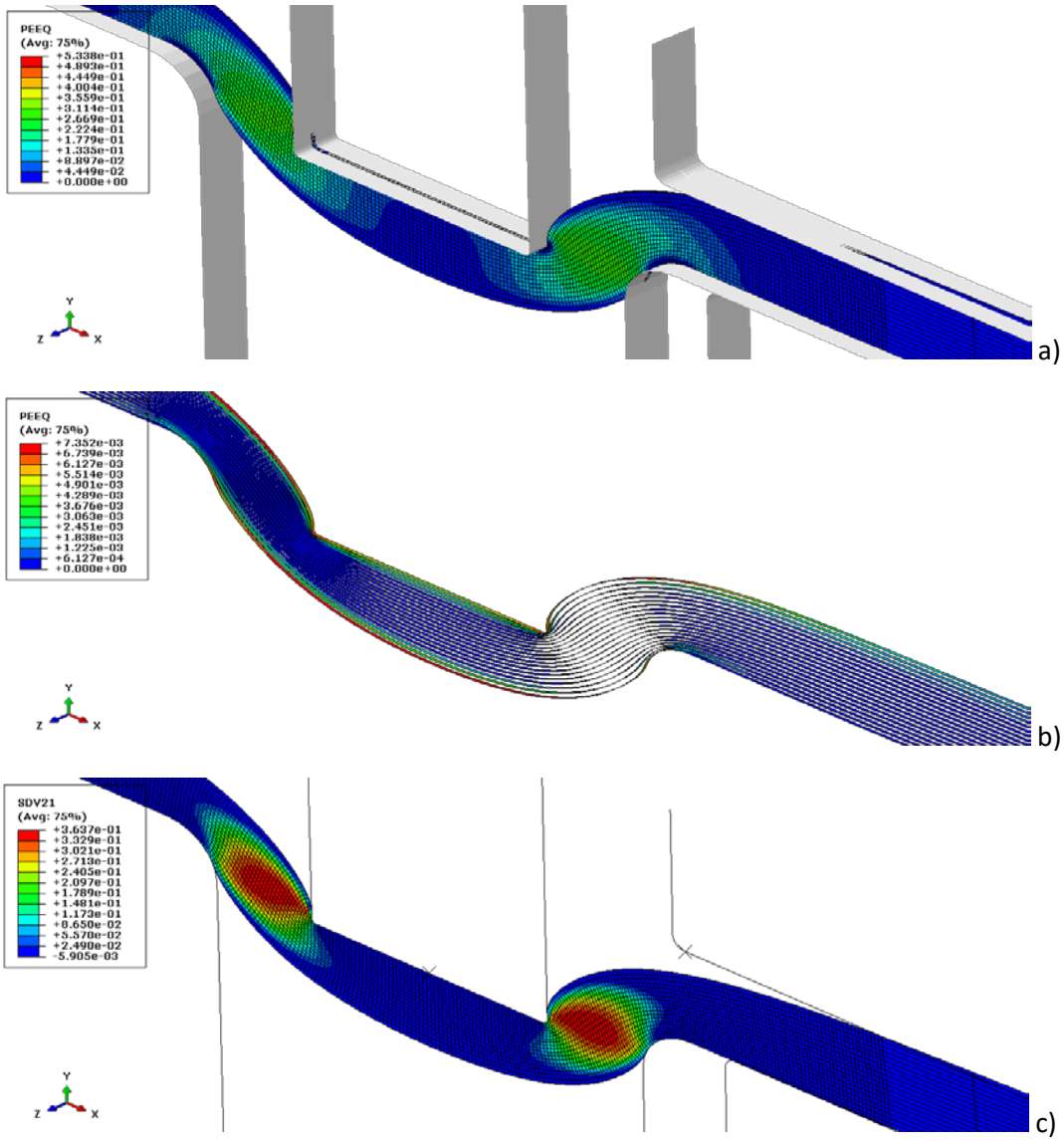

Figure 15 - Equivalent plastic strains and deformed paperboard shape at high creasing level (a). View of deformed membrane reinforcement (b). Equivalent plastic strains in the reference model (c).

Published in: Packaging Technology and Science 2017, DOI: 10.1002/pts.2298

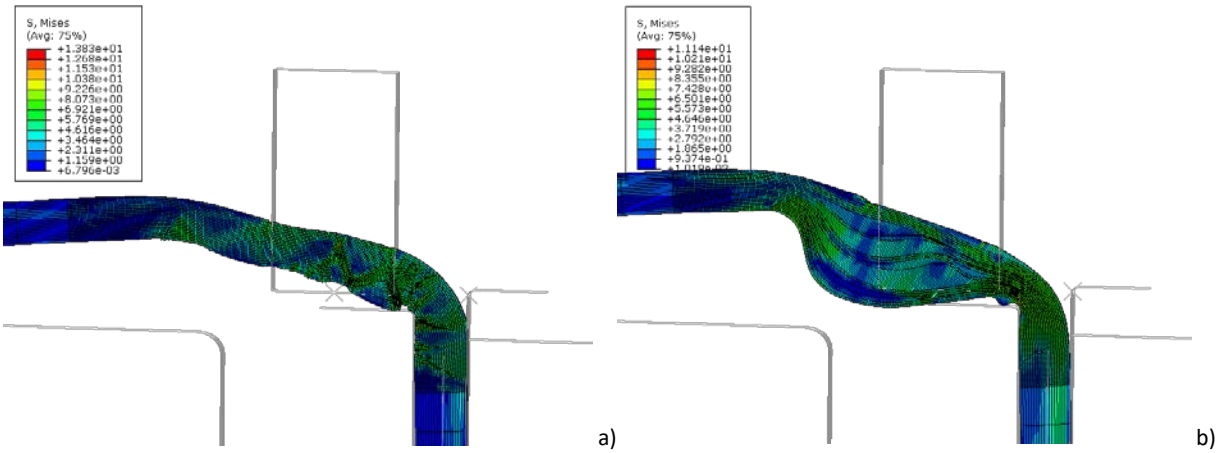

Figure 16 - Folded shape of paperboard with membrane embedded layers (a) and shells (b), with same boundary and loading conditions (90° folding).

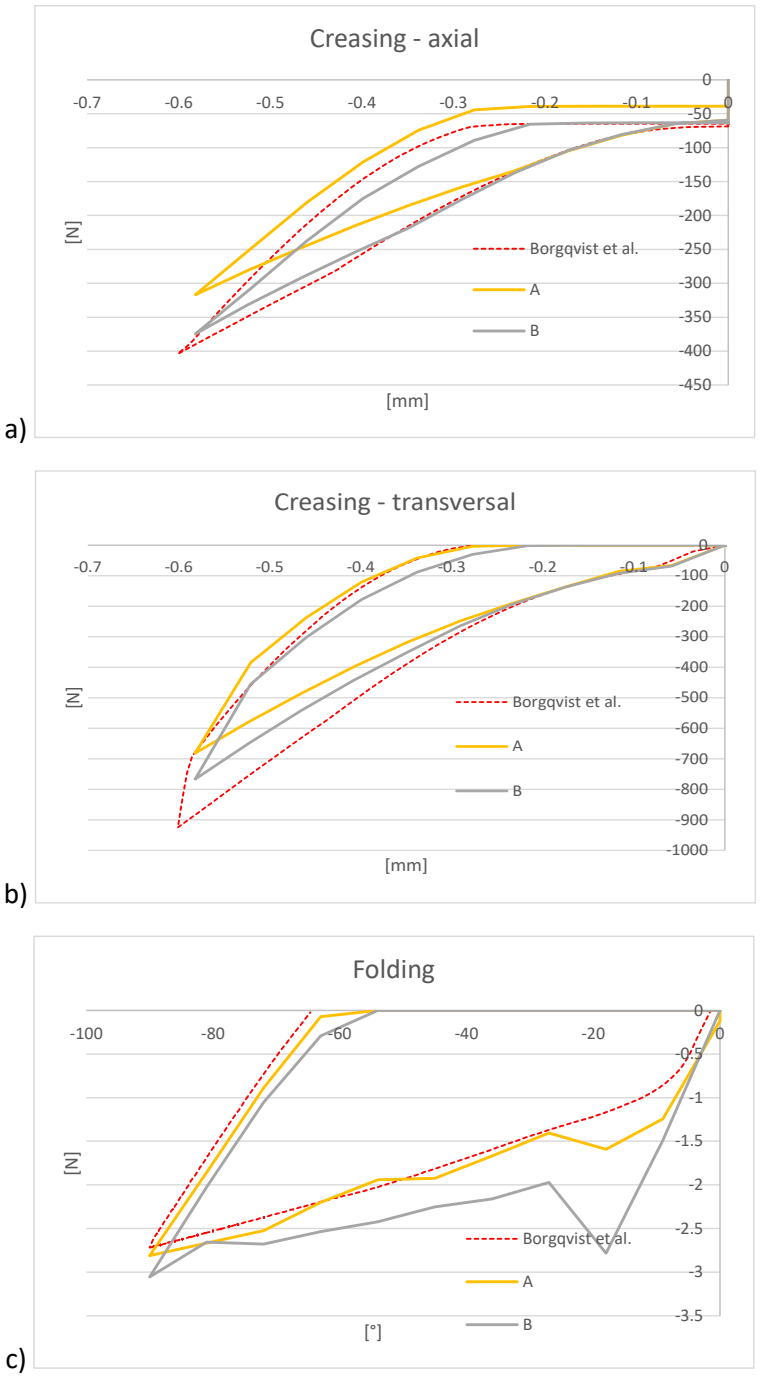

Figure 17 - Creasing axial (a) - transversal (b) forces vs transversal male displacement and folding (c) load cell force vs rotation global responses.

Published in: Packaging Technology and Science 2017, DOI: 10.1002/pts.2298

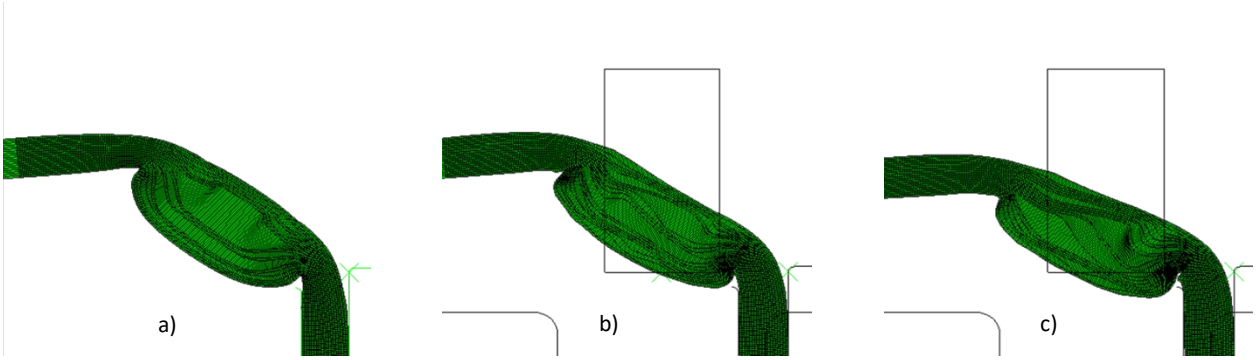

Figure 18 - Deformed shapes of target model (a) at highest level of folding (90°) in comparison with standard models "A" (b) and "B" (c).

Published in: Packaging Technology and Science 2017, DOI: 10.1002/pts.2298

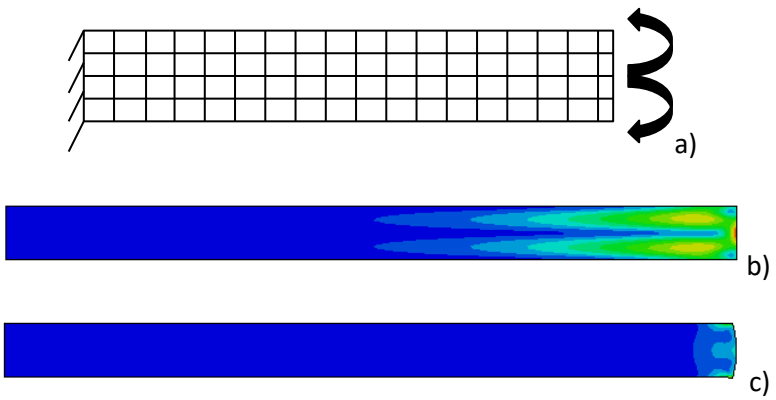

Figure 19 - Self-equilibrated loading conditions (a); linear elastic response of non-homogeneous model – von Mises stresses (b); linear-elastic response of homogeneous model – von Mises stresses (c).

Published in: Packaging Technology and Science 2017, DOI: 10.1002/pts.2298

Figure 20 - Self-equilibrated loading conditions in the paperboard FE specimen (Figure 24a), the response – von Mises stresses – of the non-linear non-homogeneous standard model "B" (a) and of the non-linear homogeneous target one (c).

Published in: Packaging Technology and Science 2017, DOI: 10.1002/pts.2298

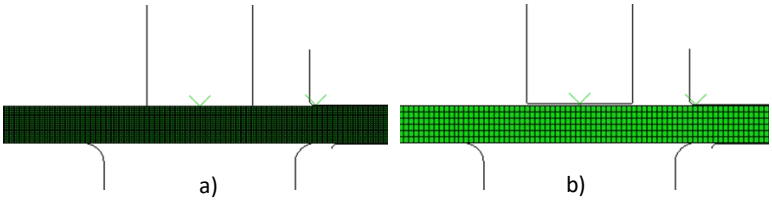

Figure 21 - Original refined (a) and unrefined (b) meshes of the laminated paperboard for the standard model.

Published in: Packaging Technology and Science 2017, DOI: 10.1002/pts.2298

a)

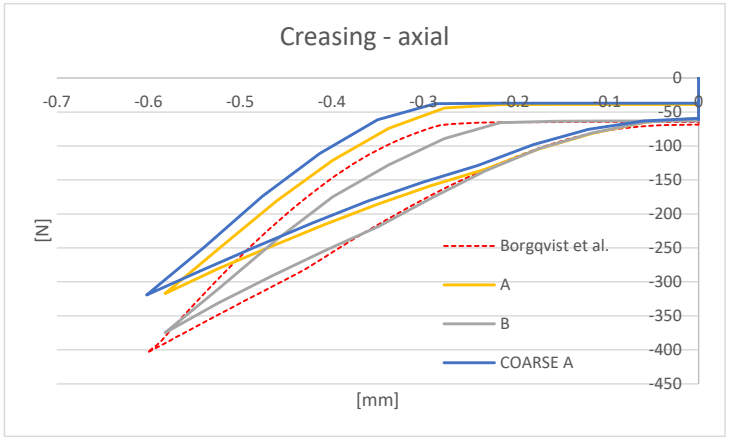

b)

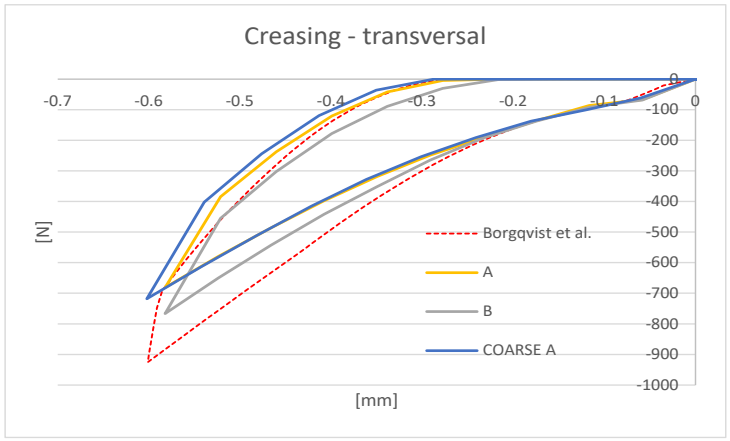

c)

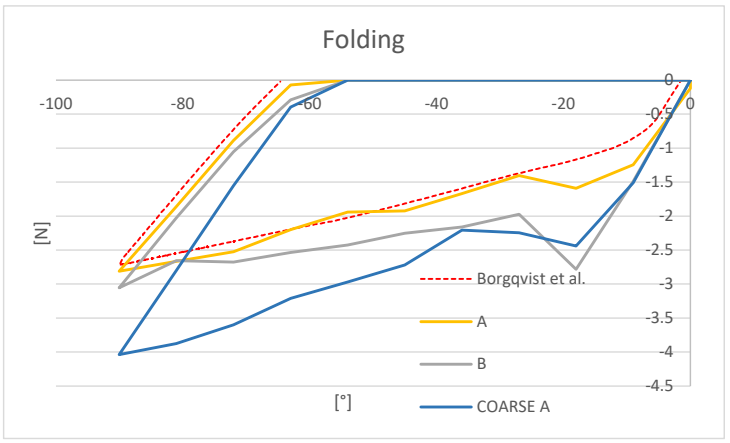

Figure 22 - Coarse mesh results. Creasing axial (a) - transversal (b) forces vs transversal male displacement and folding (c) load cell force vs rotation global responses.